MODELING BIOREMEDIATION OF CONTAMINATED GROUNDWATER

Henning Prommer and D. Andrew Barry

4

INTRODUCTION

Over the last two decades, mathematical modeling has become an important tool to assist in analyzing and understanding complex environmental systems. Wherever a multitude of processes, of either a physical, chemical, or biological nature, interact with each other, mathematical modeling provides a rational framework to formulate and integrate knowledge that has been otherwise derived from (i) theoretical work, (ii) fundamental (e.g., laboratory) investigations, and (iii) site-specific experimental work. In the case of subsurface systems, data acquisition is typically very expensive, especially in the field, so data sets are usually sparse. Thus, validation of complex models can be difficult. At the same time, it is the lack of spatially and temporally dense information and the need to fill the gaps between measured data that provide an important driving force for integrated modeling.

Henning Prommer, Department of Earth Sciences, Faculty of Geosciences, University of Utrecht, P.O. Box 80021, 3508 TA Utrecht, The Netherlands, and CSIRO Land and Water, Private Bag No. 5, Wembley WA 6913, Australia. *D. Andrew Barry*, Contaminated Land Assessment and Remediation Research Centre, Institute for Infrastructure and Environment, School of Civil Engineering and Electronics, University of Edinburgh, Edinburgh EH9 3JL, Scotland, United Kingdom.

In situ processes making use of bioremediation are prime candidates for an integrated modeling approach. Whether microbial activity is responsible for direct breakdown of organic contaminants (such as dissolved petroleum products) or whether it is employed more indirectly to alter geochemical conditions (such that metal precipitation, for example, occurs), it is evident that predictions of the combined biogeochemical-hydrodynamic system become very difficult if isolated aspects of the total problem are considered separately. The purpose of this chapter is to show how such processes can be dealt within a single comprehensive yet realistic framework.

We have previously reviewed modeling of the fate of oxidizable organic contaminants in groundwater (9) and the physical and reactive processes during biodegradation of hydrocarbons in groundwater (50). Here, we provide an introduction and overview of the mathematical/mechanistic descriptions of the important processes governing bioremediation, considering the critical factors of microbial processes (growth and decay of bacteria) and physical processes (advection and dispersion) as they relate to the applicability of bioremediation to the removal of organic pollutants from contaminated groundwater.

Bioremediation: Applied Microbial Solutions for Real-World Environmental Cleanup
Edited by Ronald M. Atlas and Jim C. Philp © 2005 ASM Press, Washington, D.C.

ROLE OF MODELING BIOREMEDIATION PROCESSES

Both passive and enhanced (active) in situ bioremediations are cost-effective contaminant cleanup methods compared to other methods such as landfill disposal or incineration (see Table 1.3). However, traditional methods are still, in many cases, the preferred remediation option despite the apparent economic benefits of bioremediation (29). Certainly, one important reason for this is the lack of reliable a priori predictions concerning the feasibility, duration, and cost of bioremediation. Site managers dealing with soil or aquifer contamination are faced with such questions as:

- To what extent will environmentally important receptors down gradient of the source zone be impacted by a contaminant?
- What are the expected average and maximum concentration levels?
- What are the timescales for cleanup to below given limits for different remediation schemes?
- What is the optimal design (in a multiobjective environment) of a particular (active/passive) remediation scheme?
- What is the sensitivity of, say, the duration of the remediation process to changes in physical or biogeochemical conditions?
- What is the probability of failure of the proposed remediation scheme?

The role of modeling in a remediation investigation is more than that of gaining an increased quantitative understanding of the biological system. The process of developing a clearly formulated conceptual model at the beginning of the modeling process (or its ongoing revision) often leads ultimately to a more rigorous scientific understanding for model developers and users. An additional and important benefit of modeling is, of course, its predictive capability. However, such predictions do bear, to a variable degree, uncertainty that originates from the following:

- incomplete hydrogeological and hydrogeochemical site characterization,
- incomplete process understanding, and
- parameter ambiguity due to spatial and/or temporal scaling issues.

Predictive modeling must therefore be viewed with appropriate caution. Given that the modeling framework is sufficiently comprehensive, issues such as parameter uncertainty can be implemented into the framework and directly quantified. The approach also contributes to the broader question of probabilistic risk assessment, which often guides engineering design of remediation schemes.

In general, modeling provides the best means to incorporate observed data into a systematic site investigation or, where data are lacking, to investigate quickly a suite of scenarios that assist in gaining a better understanding of factors dominating the duration and effectiveness of site cleanup. Below, an overview of some of the mathematical descriptions and modeling approaches involved in the simulation of bioremediation problems is provided. For the sake of clarity, we will focus initially on the quantitative description of biochemical processes (as a function of time) in batch-type systems. The following discussion of batch-type modeling uses simple examples to discuss some of the common concepts needed to model microbially mediated biodegradation reactions (9). This discussion of biotic processes will be succeeded by an introduction to some of the fundamentals of modeling physical transport before we move on to biogeochemical transport, in which these biotic and physical processes are combined.

MODELING BIOTIC REACTIVE PROCESSES

In order to be able to design active bioremediation systems and to understand passive bioremediation (natural attenuation), mechanistic descriptions that quantify microbial activity are needed. Since both the rate of microbial growth and the rate of contaminant utilization are highly dependent on the amount of biomass available to catalyze the reactions (38), such models must have the capability to pre-

dict both transient and spatial variations in biomass. To model the production of biomass and the related consumption and production of other chemicals, the key steps are (i) to determine the stoichiometry of the biodegradation reactions and, in order to describe the temporal variations, (ii) to formulate the rate expressions for the reaction kinetics. Below, we describe modeling of biodegradation under oxidizing conditions. (Note: for simplicity we do not describe here biodegradation reactions in which the contaminants act as electron acceptors.)

Biodegradation Reactions for Oxidizable Organic Contaminants

The electron flow in microbially mediated redox reactions that mineralize, e.g., petroleum hydrocarbons might be simplified into two (sub)steps. In the first step, which is the oxidation of an organic substrate, electrons are transferred to electron carriers such as NADH (14, 53). For example, the complete mineralization of toluene coupled to the reduction of NAD^+ can be written as

$$C_7H_8 + 36\ NAD^+ + 21\ H_2O \rightarrow 36\ NADH + 36\ H^+ + 7\ H_2CO_3 \quad (1)$$

In this step, electrons are gained, which can now be further transferred (14) to extracellular electron acceptors (for example, oxygen or nitrate) or, alternatively, used for the formation of additional biomass. The electron transfer to extracellular electron acceptors is referred to as respiration and involves the (re)oxidation of NADH. The appropriate reactions for the major electron accepting processes are listed in Table 4.1. In the second step, the free energy gained in these reactions can then be stored as ATP and, together with NADH, reinvested to generate new biomass. If a simplified chemical composition for biomass ($C_5H_7O_2N$) is assumed, the reaction, which diverts the electron flow towards the generation of new biomass, is described by (53):

$$10\ NADH + 5\ H_2CO_3 + NH_4^+ + 9\ H^+ + \text{free energy} \rightarrow C_5H_7O_2N + 10\ NAD^+ + 13\ H_2O \quad (2)$$

The efficiency of the microorganisms determines the fraction of electrons (gained in the oxidation step described by equation 1) that is diverted either to biomass generation according to equation 2 or towards the electron-accepting step according to the reactions listed in Table 4.1. The lower the efficiency of the bacteria, the lower the fraction of organic carbon that is incorporated into biomass and the higher the fraction that is converted to carbon dioxide. Efficiencies can vary over a wide range, depending on both organic substrates and electron acceptors, as well as the ambient conditions, such as temperature. For the reactions which yield the most energy, i.e., oxygen and nitrate reduction, efficiencies can be as high as 50 to 70%. On the other hand, they can be as low as 5%, as found for CO_2 fixation (53). Edwards et al. (22), for example, used ^{14}C-labeled substrate to investigate the degradation of toluene and xylene under sulfate-reducing conditions and found that only 10% of the organic carbon was converted to cell material, while the

TABLE 4.1 Electron-accepting processes

Electron-accepting reaction
$O_2 + 2\ NADH + 2\ H^+ \rightarrow 2\ H_2O + 2\ NAD^+ + \text{free energy}$
$2\ NO_3^- + 5\ NADH + 7\ H^+ \rightarrow N_2 + 6\ H_2O + 5\ NAD^+ + \text{free energy}$
$SO_4^{2-} + 4\ NADH + 5\ H^+ \rightarrow HS^- + 4\ H_2O + 4\ NAD^+ + \text{free energy}$
$FeOOH + NADH + 3\ H^+ \rightarrow Fe^{2+} + 2\ H_2O + NAD^+ + \text{free energy}$
$MnO_2 + 2\ NADH + 4\ H^+ \rightarrow Mn^{2+} + 2\ H_2O + 2\ NAD^+ + \text{free energy}$
$CO_2(g) + 8\ H^+ + 8\ NADH \rightarrow CH_4(g) + 2\ H_2O + 8\ NAD^+ + \text{free energy}$

rest was used as an energy source and converted to carbon dioxide. In addition to an experimentally based determination of microbial efficiency, it might also be determined from thermodynamic considerations by the method proposed by Van Briesen and Rittmann (59). On the basis of a known or estimated efficiency, the redox reactions can then be balanced. For example, in the above-mentioned case (toluene mineralization under aerobic conditions) an efficiency estimate of 60% leads to the following reaction, in which 40% of the organic carbon (C_7H_8) is converted to inorganic carbon (HCO_3^-) and 60% is converted to biomass ($C_5H_7O_2N$):

$$C_7H_8 + 0.84\ NH_4^+ + 4.8\ O_2 + 0.48\ H_2O \rightarrow 2.8\ HCO_3^- + 0.84\ C_5H_7O_2N + 3.64\ H^+ \quad (3)$$

For the oxidation/mineralization of toluene under sulfate-reducing conditions, assuming a lower (10%) efficiency, balancing leads to

$$C_7H_8 + 0.14\ NH_4^+ + 4.15\ SO_4^{2-} + 2.58\ H_2O + 1.86\ H^+ \rightarrow 6.30\ HCO_3^- + 0.14\ C_5H_7O_2N + 4.15\ H_2S \quad (4)$$

Under the same assumptions, but for a different reducible, organic compound (benzene), one obtains

$$C_6H_6 + 0.12\ NH_4^+ + 3.45\ SO_4^{2-} + 2.64\ H_2O + 1.38\ H^+ \rightarrow 5.4\ HCO_3^- + 0.12\ C_5H_7O_2N + 3.45\ H_2S \quad (5)$$

whereas the same exercise for ethylbenzene and xylene(s) leads to

$$C_8H_{10} + 0.16\ NH_4^+ + 2.52\ H_2O + 2.34\ H^+ \rightarrow 7.2\ HCO_3^- + 0.16\ C_5H_7O_2N + 4.85\ H_2S \quad (6)$$

Reactions 3 to 6 and their stoichiometry reflect the conditions for microbial growth. If cell growth is neglected, the stoichiometry of the mineralization reaction simplifies, for example, from reaction 4 to

$$C_7H_8 + \mathbf{4.5}\ SO_4^{2-} + \mathbf{3}\ H_2O + \mathbf{2}\ H^+ \rightarrow \mathbf{7}\ HCO_3^- + \mathbf{4.5}\ H_2S \quad (7)$$

In this reaction, there is obviously more sulfate consumed than in reaction 4, which considers microbial growth (4.5 versus 4.15 mol of sulfate per mol of toluene degraded). This apparent discrepancy can be accounted for by noting the concentrations and valence of the redox-sensitive reactants before and after the reaction. For the complete mineralization of toluene, electron balance requires (50)

$$Y_{C_7H_8} o\nu_{C_7H_8} + Y_{SO_4^{2-}} o\nu_{SO_4^{2-}} = Y_{HCO_3^-} o\nu_{HCO_3^-} + Y_{H_2S} o\nu_{H_2S} \quad (8)$$

where $Y_{C_7H_8}$, $Y_{SO_4^{2-}}$, $Y_{HCO_3^-}$, and Y_{H_2S} are the stoichiometric factors of toluene, sulfate, bicarbonate, and hydrogen sulfide, respectively, and $o\nu_{C_7H_8}$, $o\nu_{SO_4^{2-}}$, $o\nu_{HCO_3^-}$, and $o\nu_{H_2S}$ are the appropriate valences of these species. Maintaining mass balance for sulfur and carbon requires that $Y_{SO_4^{2-}} = Y_{H_2S}$ and $Y_{HCO_3^-} = 7$, respectively. Consideration of microbial growth mandates that ammonium and bacteria are included in the electron balance:

$$Y_{C_7H_8} o\nu_{C_7H_8} + Y_{SO_4^{2-}} o\nu_{SO_4^{2-}} + Y_{NH_4^+} o\nu_{NH_4^+} = Y_{HCO_3^-} o\nu_{HCO_3^-} + Y_{C_5H_7O_2N}\, o\nu Y_{C_5H_7O_2N} + Y_{H_2S}\, o\nu_{H_2S} \quad (9)$$

where $Y_{NH_4^+}$ and $Y_{C_5H_7O_2N}$ are the stoichiometric factors for ammonium and bacteria, respectively, and $o\nu_{NH_4^+}$ and $o\nu_{C_5H_7O_2N}$ are the corresponding valences (50). However, nitrogen balance requires that

$$Y_{NH_4^+} = Y_{C_5H_7O_2N} \quad (10)$$

At the same time, bacteria and ammonium have the same valence, in which case it turns out that the respective terms are equivalent. Thus, the difference in sulfate consumption between the case described by reaction 4 and the corresponding case described by reaction 7 can be calculated from (50):

$$\Delta Y_{SO_4^{2-}} = \frac{(7-6.3)ov_{HCO_3^-}}{ov_{SO_4^{2-}} - ov_{H_2S}} = \frac{0.7 \times 4}{6-(-2)} = 0.35 \quad (11)$$

As we will see, the electron acceptor "saving" that occurs during this step might subsequently be consumed during microbial decay. The reaction for the decay of bacteria (under sulfate-reducing conditions) and the corresponding consumption of electron acceptors is described by (50):

$$C_5H_7O_2N + 3\ H_2O + 2.5\ SO_4^{2-} \rightarrow 5\ HCO_3^- + 2.5\ HS^- + 1.5\ H^+ + NH_4^+ \quad (12)$$

It follows from the stoichiometry of the reaction that the decay of 1 mol of bacteria ($C_5H_7O_2N$) requires 2.5 mol of sulfate. Consequently, the decay of the 0.14 mol of bacteria produced during growth (see reaction 4) consumes $0.14 \times 2.5 = 0.35$ mol of sulfate. This amount equals the difference in sulfate consumption between reactions 4 and 7. Accordingly, where microbial concentrations become steady state or quasi-steady state, i.e., where microbial growth occurs at the same rate as bacterial decay, the stoichiometry from reaction 7 applies. Depending, for example, on whether the assumption of a quasi-steady-state microbial concentration is a sufficiently good approximation for a given problem, kinetic reaction models of different complexities can be built on the basis of the above stoichiometric relationships.

Rate expressions for the mineralization reactions typically used in reactive transport models for biodegradation are based on three conceptual reaction models. In the first and simplest model (13), the biodegradation reaction is assumed to be instantaneous. This means that the reaction is limited only through the availability of either the electron acceptor or the contaminant (electron donor). The reaction is assumed to proceed at an infinite rate until either of these is depleted. A widely used biodegradation model that incorporates this approach for aerobic (only) biodegradation of hydrocarbons is BIOPLUME (13, 51), and an analytical solution for this problem was provided by Ham et al. (30). Note that in this approach, bacterial concentrations are not modeled explicitly. This assumption is, however, not necessarily suitable for simulating slowly degrading hydrocarbon contaminants. An improved description of the reaction kinetics, using a dual-substrate Monod kinetics formulation, was proposed previously (52). In this description, the biomass concentration is assumed to remain constant with time (although it can vary spatially) throughout the subsurface (i.e., model domain). The modeling approach described by Lu et al. (39) also incorporates this assumption but provides a framework that allows the simulation of multiple electron-accepting processes. In many cases, however, it is obvious that the dynamics of biomass growth will play an important role in biodegradation. Hence, in the most realistic description of the bioremediation process, the contaminant degradation kinetics are typically described by using Monod kinetics, and the biomass concentration is allowed to change as a function of space and time as the biomass grows and decays.

Microbial Growth and Decay

In the macroscopic mathematical descriptions of microbial growth dynamics aimed at governing laboratory- or field-scale processes, many of the complex interdependencies that are known at the microscopic scale are commonly neglected and described by empirical formulations based on the classical works of Michaelis and Menten (41) and Monod (42). The expression describing a specific bacterial growth rate, v_{sp}, observed in many batch experiments is:

$$v_{sp} = v_{max} \frac{C_{org}}{K_{org} + C_{org}} \quad (13)$$

where C_{org} is the concentration of the organic substrate, v_{max} is an asymptotic maximum specific uptake rate, and K_{org} is the half-saturation constant, the substrate concentration at which the actual uptake rate equals $v_{max}/2$. Based on equation 13, the total uptake rate v_m considers the dependency of the change of microbial mass on the actual microbial concentration X itself:

$$v_m = v_{max} \frac{C_{org}}{K_{org} + C_{org}} X \quad (14)$$

An additional (potential) growth limitation by electron acceptor availability might be incorporated into equation 14, leading to

$$v_m = v_{max} \frac{C_{org}}{K_{org} + C_{org}} \frac{C_{ea}}{K_{ea} + C_{ea}} X \quad (15)$$

where C_{ea} is the electron acceptor concentration and K_{ea} is the appropriate half-saturation constant (3,4). The complete mass balance equation for the microbial mass, X, describing the change of microbial concentration as a function of time, also needs to include microbial decay:

$$\frac{\partial X}{\partial t} = \frac{\partial X_{growth}}{\partial t} + \frac{\partial X_{decay}}{\partial t} \quad (16)$$

with

$$\frac{\partial X_{growth}}{\partial t} = v_{max} Y_x \frac{C_{org}}{K_{org} + C_{org}} \frac{C_{ea}}{K_{ea} + C_{ea}} X \quad (17)$$

and

$$\frac{\partial X_{decay}}{\partial t} = -v_{dec} X \quad (18)$$

where v_{dec} is a decay rate constant and Y_x is a stoichiometric factor. During growth ($v_m > 0$), both organic substrate and electron acceptors are consumed at rates that are proportional to v_m. Thus, for a known reaction stoichiometry, the actual rates can be easily determined. For example, in the previously discussed case of toluene degradation under sulfate-reducing conditions (equation 4), the complete mineralization of 1 mol of toluene consumes 4.15 mol of sulfate (during growth) and yields 0.14 mol of sulfate-reducing bacteria (SRB), thus:

$$\frac{\partial X_{growth}}{\partial t} = 0.14 v_m \quad (19)$$

and

$$\frac{\partial C_{sulf}}{\partial t} = -4.15 v_m \quad (20)$$

where C_{sulf} is the concentration of sulfate. As shown in Fig. 4.1, for given initial concentrations (at time $t = 0$ [see Table 4.2]), we can now compute the temporal development of toluene and sulfate and of the microbial mass in a closed batch-type system (case 1a). This can be done, for example, with the geochemical model PHREEQC-2 (45) by using its capability to compute arbitrary user-defined kinetic reactions. Notable in the upper plot is the lag period of several days before the degradation affects the aqueous concentrations of toluene and sulfate. Its length depends largely on the initial bacterial concentration and on v_{max}, the maximum uptake rate (values given in Tables 4.2 and 4.3). The removal of the initial toluene mass (0.1 mmol) is reached after 14 days, at a time when approximately 0.415 mmol of sulfate is depleted. The microbial (net) growth then stops immediately ($v_m = 0$) and the microbial mass is subsequently changing at the rate given by equation 18, thereby consuming the remaining 0.035 mmol of sulfate, as discussed previously (Fig. 4.1, case 1a). By comparison, Fig. 4.1 shows also the temporal development of the sulfate concentration if the effects of the different valence states of bacteria (compared to the end product CO_2) and the related geochemical changes are not considered (Fig. 4.1, case 1b). In the latter case, all sulfate is consumed during bacterial growth and none

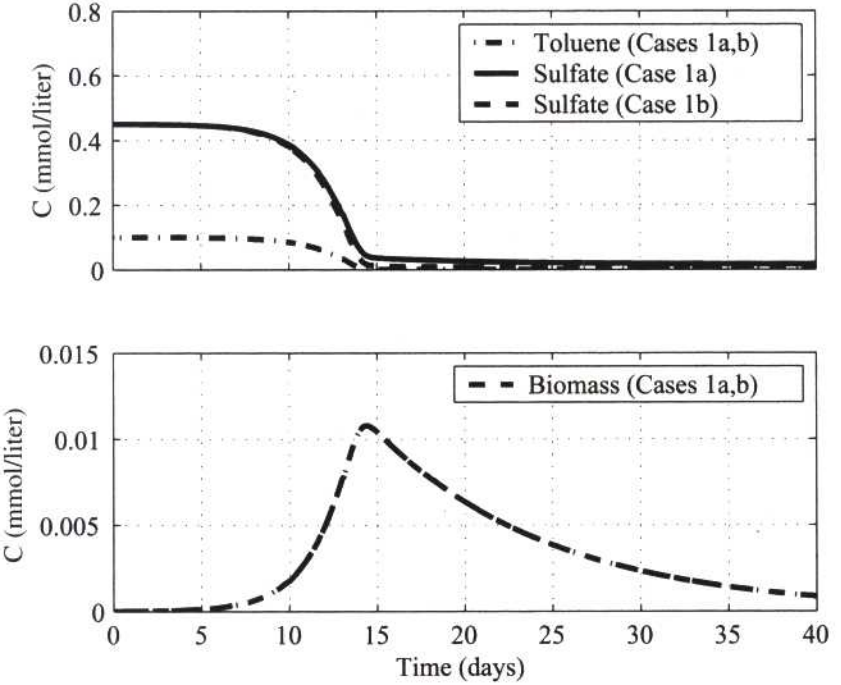

FIGURE 4.1 Simulation of toluene mineralization by SRB in a closed batch system.

TABLE 4.2 Initial concentrations of aqueous components and minerals in the batch-type biodegradation simulations

Aqueous component	Initial concn (mol/liter)				
	Case 1	Case 2	Case 3	Case 4	Case 5
Benzene	—[b]	4.0×10^{-4}	—	—	—
Toluene	1.0×10^{-4}	3.0×10^{-4}	3.0×10^{-4}	3.0×10^{-4}	2.0×10^{-4}
Ethylbenzene	—	1.0×10^{-4}	—	—	—
Xylene	—	2.5×10^{-4}	—	—	—
O(0)	—	—	6.25×10^{-4}	—	6.25×10^{-4}
N[a]	1.0×10^{-4}	1.0×10^{-4}	5.0×10^{-4}	1.0×10^{-4}	5.0×10^{-4}
S(6)	4.5×10^{-4}	5.0×10^{-3}	8.0×10^{-4}	1.0×10^{-3}	—
C(4)	—	—	—	—	1.12×10^{-3}
Ca	—	—	—	—	3.32×10^{-3}
Na	—	—	—	—	1.00×10^{-3}
Cl	—	—	—	—	6.17×10^{-3}
Aerobes	—	—	1.0×10^{-8}	—	—
Denitrifiers			1.0×10^{-8}		
SRB	1.0×10^{-8}	1.0×10^{-8}	1.0×10^{-8}	1.0×10^{-8}	—
Calcite	—	—	—	—	1.0×10^{-3}
$Fe(OH)_3(a)$	—	—	—	—	4.0×10^{-3}
Siderite	—	—	—	—	0

[a] Total nitrogen, except for cases 3 and 5, where it is defined as nitrate/N (5).
[b] —, not considered in simulation.

TABLE 4.3 Parameters used in the batch-type biodegradation modeling (cases 1 to 5)

Aqueous component	Value for:				
	Case 1	Case 2	Case 3	Case 4	Case 5
K_{ox} (mol liter^{-1})	—[a]		1.0×10^{-5}	—	1.0×10^{-5}
K_{nit} (mol liter^{-1})	—	—	—	—	1.0×10^{-5}
K_{sulf} (mol liter^{-1})	1.0×10^{-5}	1.0×10^{-5}	1.0×10^{-5}	1.0×10^{-5}	—
$K_{Fe(OH)_3}$ (mol liter^{-1})	—	—	—	—	1.0×10^{-5}
K_N (mol liter^{-1}	—	—	2.0×10^{-6}	—	—
$K_{benzene}$ (mol liter^{-1}	—	1.0×10^{-5}	—	—	—
$K_{toluene}$ (mol liter^{-1})	1.0×10^{-5}	1.0×10^{-5}	1.0×10^{-5}	1.0×10^{-5}	—
$K_{ethylbenzene}$ (mol liter^{-1})	—	1.0×10^{-5}	—	—	—
K_{xylene} (mol liter^{-1})	—	1.0×10^{-5}	—	—	—
$K_{inhib,\ ox}$ (mol liter^{-1})	—	—	5.0×10^{-6}	—	—
$K_{inhib,\ bio}$ (mol liter^{-1})				1.0×10^{-4}	—
				2.5×10^{-5}	
				1.0×10^{-5}	
				2.5×10^{-6}	
$\nu_{max,\ sulf,\ benzene}$ (day^{-1})	—	0.1	—	—	—
$\nu_{max,\ herob,\ toluene}$ (day^{-1})	—	—	10.0	—	—
$\nu_{max,\ sulf,\ toluene}$ (day^{-1})	5.0	5.0	5.0	5.0	—
$\nu_{max,\ sulf,\ ethylbenzene}$ (day^{-1})	—	0.5	—	—	—
$\nu_{max,\ sulf,\ xylene}$ (day^{-1})	—	1.0	—	—	—
ν_{decay} (day^{-1})	0.1	0.1	0.1	0.1	0.1
r_{ox} (day^{-1})	—	—	—	—	4.32×10^{-5}
r_{nit} (day^{-1})	—	—	—	—	8.64×10^{-6}
$r_{Fe(OH)_3}$ (day^{-1})	—	—	—	—	8.64×10^{-7}

[a] —, not considered in simulation.

is consumed during bacterial decay. Note that the differences between the two cases become more pronounced with increasing bacterial efficiency (here 10%), as shown for example by Barry et al. (9) for simulations involving dissolved organic carbon, CH_2O, and oxygen.

Of course, the formulations for microbial growth above apply only to the uptake of a single substrate, whereas contamination often involves numerous (organic) compounds. The (possibly simultaneous) uptake of these substrates can be incorporated into the modeling approach described above. The model of Kindred and Celia (35), also used in other studies (24, 48, 55), states that the growth of the degrading microbial community is simply the sum of the growth rates arising from degradation of individual organic contaminants:

$$\frac{\partial X}{\partial t} = \left[\left(\sum_{n=1,\, n_{org}} \frac{\partial X_n}{\partial t} \right) - \nu_{dec} \right] X \qquad (21)$$

where, in analogy to equation 17, each of the growth terms $\partial X_n/\partial t$ can be derived from

$$\frac{\partial X_n}{\partial t} = \nu^n_{max} Y_x \frac{C_{org,\,n}}{K_{org,\,n} + C_{org,\,n}} \frac{C_{ea}}{K_{ea} + C_{ea}} \qquad (22)$$

The uptake rates ν^n_{max} can differ between different substrates. In this way, it is possible to model varying degradation rates of different electron donors. This can be necessary when, for example, benzene degrades more slowly than the other compounds, as reported by Davis et al. (19). The case of a simultaneous uptake of BTEX constituents (benzene, toluene, ethylbenzene, xylenes) by one microbial group is demonstrated by the next simulation example (case 2). Different initial amounts of organic compounds were assumed to be present (Table 4.2) and the initial sulfate mass was increased compared to that of the first example (thus, still present in excess). As can be seen in Fig. 4.2, for the chosen parameters

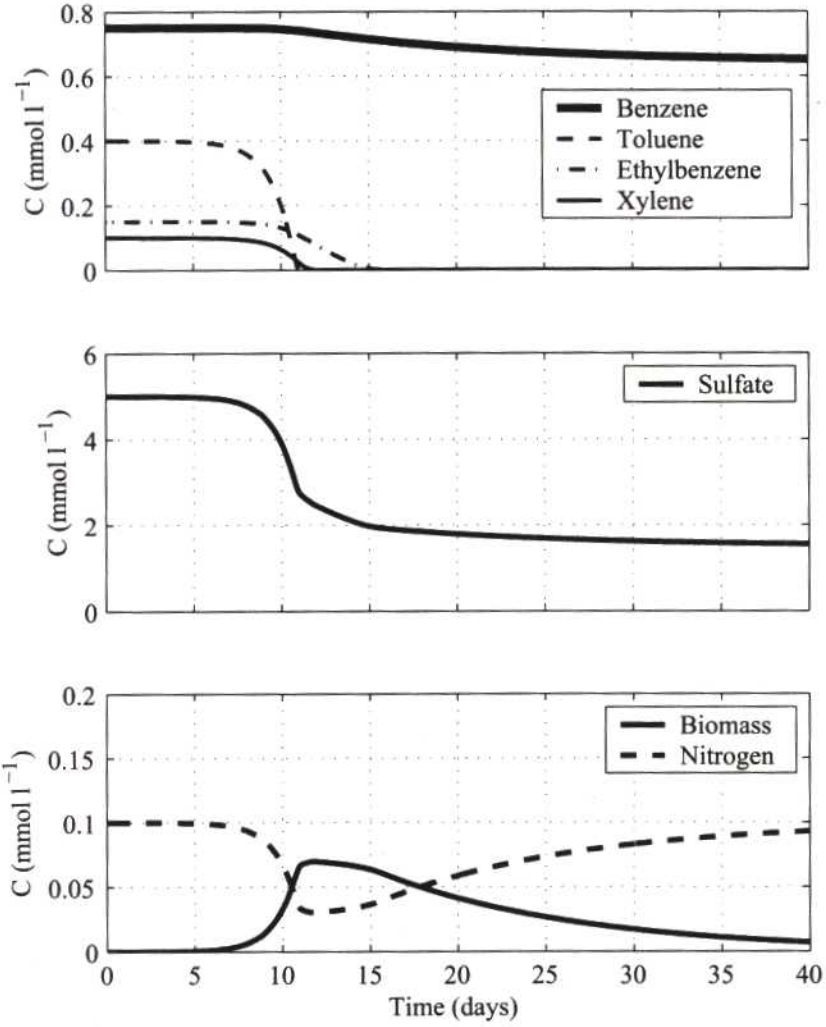

FIGURE 4.2 Simulation of BTEX mineralization by SRB in a closed batch system (after the work of Barry et al. [9]).

(Table 4.3), toluene and ethylbenzene degrade first. They are followed by xylene, while degradation of benzene takes longest. The rate of sulfate consumption decreases once toluene and ethylbenzene are depleted and slows down further as soon as only benzene is left to degrade. Figure 4.2 shows also the temporal development of the nitrogen concentration within the aqueous phase. During bacterial growth, nitrogen is removed from the aqueous phase and incorporated into biomass. Once the bacterial decay rate exceeds the growth rate, the nitrogen released to the aqueous phase eventually returns the nitrogen concentration to its initial value.

Nutrient Limitation

While in many cases bacterial activity is limited by substrate or electron acceptor availability, growth might also be limited by nutrients such as nitrogen or phosphorus. The most common mathematical model to consider this effect is

simply to add an additional Monod term to equation 17. For the case of a potential growth limitation by nitrogen, this gives

$$\frac{\partial X_{\text{growth}}}{\partial t} = \nu_{\max} Y_x \frac{C_{\text{org}}}{K_{\text{org}} + C_{\text{org}}} \frac{C_{\text{ea}}}{K_{\text{ea}} + C_{\text{ea}}} \frac{C_n}{K_n + C_n} X \quad (23)$$

where K_n is a half-saturation constant for nitrogen and C_n is the concentration of nitrogen in the aqueous phase.

Multiple Bacterial Groups and Growth Inhibition

So far, we have assumed that the contaminant degradation is dominated by a single biogeochemical process in which one particular bacterial group is largely responsible for the contaminant breakdown. This assumption might indeed be valid for some cases of active bioremediation schemes in which electron acceptors are actively replenished. However, in most instances where contaminants degrade naturally, i.e., without any intervention, it is very likely that more than one bacterial group will be involved in the degradation process as electron acceptors become locally depleted. When this is the case, bacterial groups that rely on less thermodynamically favorable electron acceptors might take over and proceed with the contaminant breakdown. Eventually this leads in most cases to the formation of distinct redox zones whereby the dominating bacterial group corresponds to the most thermodynamically favorable electron acceptor within each zone. In numerical models, the sequential use of electron acceptors can be achieved through the introduction of additional Monod-type inhibition terms. For example, the inhibited growth of sulfate-reducing bacteria in the presence of oxygen and nitrate can be expressed by

$$\frac{\partial X_{\text{sulf}}}{\partial t} = \nu_{\text{sulf}}^{\max} Y_x I_{\text{inh,ox}} I_{\text{inh,nit}} \frac{C_{\text{org}}}{K_{\text{org}} + C_{\text{org}}} \frac{C_{\text{sulf}}}{K_{\text{sulf}} + C_{\text{sulf}}} X_{\text{sulf}} \quad (24)$$

and using for the inhibition terms:

$$I_{\text{inh, ox}} = \frac{K_{\text{inh, ox}}}{K_{\text{inh, ox}} + C_{\text{ox}}} \quad (25)$$

and

$$I_{\text{inh, nit}} = \frac{K_{\text{inh, nit}}}{K_{\text{inh, nit}} + C_{\text{nit}}} \quad (26)$$

where C_{ox} and C_{nit} are the concentrations of oxygen and nitrate, respectively, and K_{org} and K_{sulf} are half-saturation constants. $K_{\text{inh, ox}}$ and $K_{\text{inh, nit}}$ are inhibition constants that need to be much smaller than typical nitrate or oxygen concentrations under ambient conditions. The Monod-type inhibition term $I_{\text{inh, ox}}$ will then remain ≈ 0 as long as oxygen is present in significant amounts but reaches its maximum value of ≈ 1 as soon as oxygen is depleted. Growth of SRB remains inhibited after $I_{\text{inh, ox}}$ becomes ≈ 1, because $I_{\text{inh, nit}}$ is still ≈ 0 as long as nitrate is present. Once nitrate concentrations become very low, $I_{\text{inh, nit}}$ also approaches ≈ 1 and growth of SRB can start to increase to rates that will affect the concentration of the organic substrate (no more growth inhibition). Mathematically, the form of the inhibition terms resembles that used in model approaches that do not explicitly consider bacterial growth and decay for the computation of the oxidation rates of the organic compounds (39). Van Cappellen et al. (60) have used inhibition terms of this form for the simulation of the oxidation of organic matter in aquatic sediments. Most comprehensive biodegradation models incorporate multiple inhibition terms into the growth equation(s). Following equation 21 and assuming that microbial groups are distinguished by their capacity of using a particular electron acceptor, a generalized formulation for microbial growth is then

$$\frac{\partial X}{\partial t} = \left\{ \left[\prod_{i=1,\, n_{\text{inh}}} I_{\text{inh},\, i} \left(\sum_{n=1,\, n_{\text{org}}} \frac{\partial X_n}{\partial t} \right) \right] - \nu_{\text{dec}} \right\} X \quad (27)$$

where $I_{inh,i}$ is an inhibition term similar to that in equation 25 for each of the n_{inh} more favorable electron acceptors. An illustrative example for the sequential use of electron acceptors is given by the third simulation example (case 3). It involves the sequential consumption of oxygen, nitrate, and sulfate during oxidation of toluene. For the initial conditions and parameters chosen in this example (Table 4.2), full mineralization of toluene occurs during the course of the numerical experiment, as can be seen in Fig. 4.3. However, it can also be seen that the degradation of toluene occurs in three distinct phases, i.e., under aerobic, denitrifying, and finally sulfate-reducing conditions. During the first phase, the oxygen that is initially present in the system is consumed rapidly, subsequent to an initial lag period during which toluene concentrations remain essentially unchanged. The lag period results from the very small initial microbial concentrations of the aerobic degraders (aerobes). Once oxygen is depleted, the oxidation of toluene then continues after a further lag period. It involves the growth of denitrifying bacteria, which stops once nitrate is also depleted. In the final stage, the toluene removal is completed by the activity of the SRB.

Some conceptual models for biologically mediated degradation reactions suggest that with increasing biomass concentrations and thus increasing biofilm thickness, degradation rates might become limited by the supply of reactants. In order to avoid solving the diffusional transport of reactants at a microscopic (i.e., within-biofilm) level, Kindred and Celia (35) have proposed use of a macroscopic formulation to account for the rate limitation resulting from excessive biomass accumulation. The mass balance equation for bacteria becomes

$$\frac{\partial X}{\partial t} = (\upsilon_{max} Y_x I_{bio} \frac{C_{org}}{K_{org} + C_{org}} \frac{C_{ea}}{K_{ea} + C_{ea}} - \upsilon_{dec})X \quad (28)$$

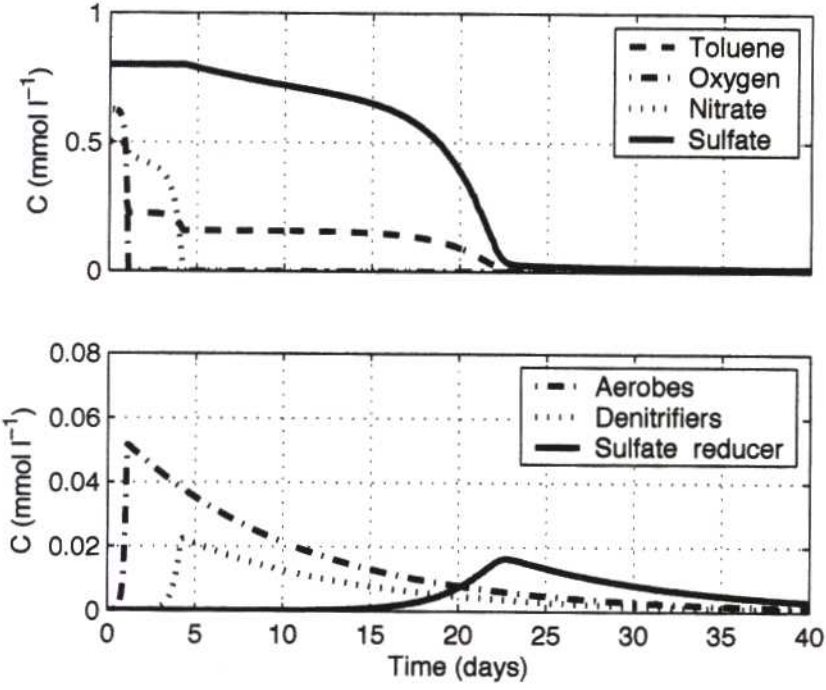

FIGURE 4.3 Simulation of toluene mineralization by sequential use of oxygen, nitrate, and sulfate in a closed batch system (after the work of Barry et al. [9]).

with:
$$I_{bio} = \frac{K_{bio}}{K_{bio} + X} \quad (29)$$

where K_{bio} is an inhibiting biomass concentration. As Kindred and Celia (35) pointed out, when a microbial concentration becomes much larger than K_{bio}, the growth term will become similar to the basic Michaelis-Menten expression. Conceptually, this represents a situation where the real biofilm thickness becomes irrelevant since the metabolic activity occurs predominantly on the upper layers of a biofilm that are more exposed to the nutrient-bearing aqueous phase. A mathematically equivalent inhibition term aimed at suppressing excessive microbial growth was proposed by Zysset et al. (69):

$$I_{bio} = \frac{\theta_{max} - X}{\theta_{max}} \quad (30)$$

where θ_{max} is a maximum bacterial concentration.

The sensitivity of modeling results to the selected magnitude of K_{bio} is illustrated by case 4 (Fig. 4.4). It can be seen that if $K_{bio} = 1 \times 10^{-4}$ mol liter^{-1}, the simulated evolution of the biomass concentrations is almost similar to

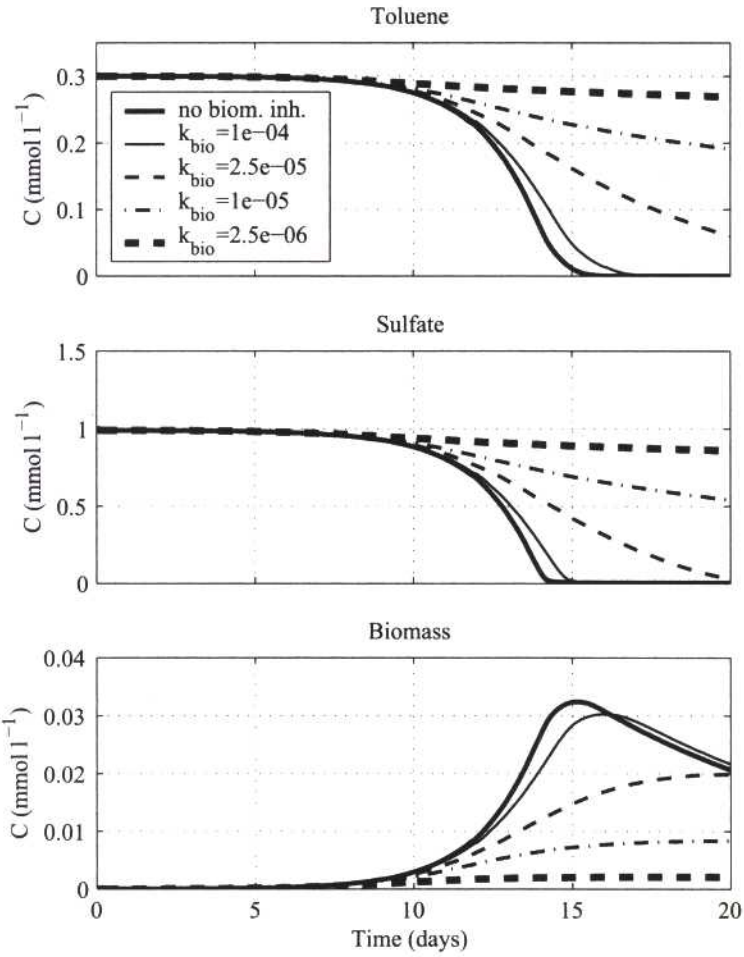

FIGURE 4.4 Simulation of toluene mineralization by sulfate with and without growth inhibition.

that of the uninhibited case. In contrast, for the example simulation that uses the smallest K_{bio} (2.5×10^{-6} mol liter^{-1}), the microbial growth is strongly inhibited, resulting in a much lower contaminant removal rate.

Modeling Geochemical Changes during Biodegradation

In many cases, the reactions that are critical in determining the rates of removal of contaminants from groundwater involve the production and consumption of protons and other reactants, which subsequently can trigger the precipitation or dissolution of minerals, ion exchange, or surface complexation reactions (21). For example, the oxidation of BTEX compounds not only consumes electron acceptors, but also causes changes in alkalinity and pH and produces reduced forms of electron acceptors such as sulfide or ferrous iron. The latter species may react further and precipitate as minerals such as siderite ($FeCO_3$), iron sulfide (FeS), or pyrite (FeS_2). For simplicity, those effects are often neglected in modeling studies.

There are situations, however, in which the simulation of only the primary reactions provides insufficient information or delivers erroneous results. Where reaction rates are dependent on the pH of the groundwater, the simulation of the hydrogeochemistry and thus of secondary reactions might be required, which itself is changing during biodegradation. When monitored natural attenuation is considered for use as a remediation technique, understanding and quantifying the detailed geochemical footprint of degradation reactions can be an important component for the successful verification of the attenuation processes (64). Given the increased use of monitored natural attenuation for treatment of BTEX-contaminated groundwater, the inclusion of the geochemical changes that occur during the bioremediation process can be essential for accurate modeling of the fate of the contaminants.

The next example that we will discuss here (case 5) provides a relatively simple illustration of a situation where geochemical interactions occur in response to the oxidation of organic compounds. As above, we use a batch-type model to look at the fate of the reaction products. Toluene mineralization is taken again as the primary reaction, which now also acts as the driving force for secondary reactions. As noted by Brun and Engesgaard (15), such problems can be modeled by a two-step method, or so-called partial equilibrium approach. This approach splits the redox reaction to be modeled into two separate steps: (i) the electron-donating oxidation step and (ii) the electron-accepting step, as discussed in earlier sections of this chapter. According to Postma and Jakobsen (47), the assumption that the first step is rate limiting is made and thus the second step can be simply modeled as an equilibrium reaction. For illustration purposes, we use, in contrast to the previous simulation examples, an approach in which microbial growth and decay are not included in the model. Instead, we use a simpler rate equation for the time-dependent degradation of toluene, based on an additive Monod expression:

$$\frac{\partial C_{org}}{\partial t} = -\sum_{i=1,\, n_{ea}} r_{ea,\,i} \frac{C_{ea,\,i}}{K_{ea,\,i} + C_{ea,\,i}} \quad (31)$$

where C_{org} is here the toluene concentration, $C_{ea,\,i}$ is the concentration of the ith electron acceptor, n_{ea} is the number of electron acceptors, and $r_{ea,\,i}$ and $K_{ea,\,i}$ are the reaction rate and the half-saturation constants corresponding to the ith electron acceptor, respectively. The form of equation 31 causes the oxidation rate of toluene to decrease successively as more and more oxidation capacity gets depleted, i.e., as redox conditions become more and more reducing. In the simulation, we assume that oxygen, nitrate, and amorphous iron oxide [$Fe(OH)_3$] are initially present as electron acceptors. The parameter values and initial concentrations used for this numerical experiment are shown in Tables 4.2 and 4.3, while the simulation results are shown in Fig. 4.5. As microbial growth and decay are not simulated, toluene degradation begins with-

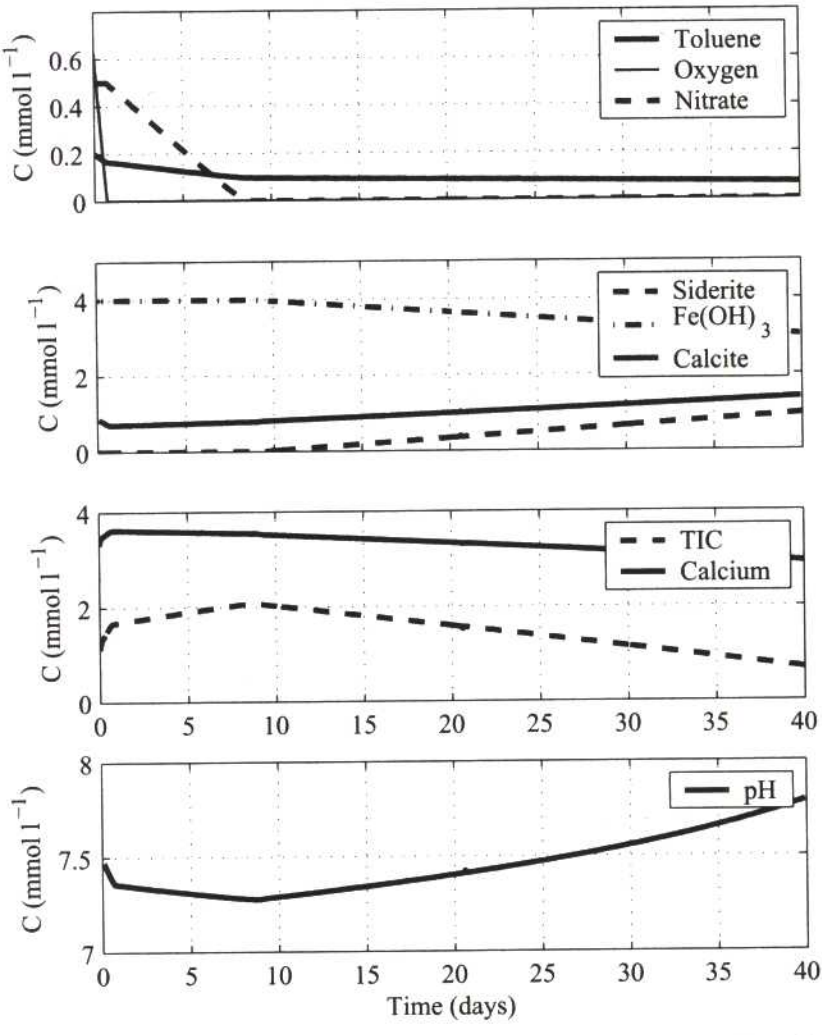

FIGURE 4.5 Simulation of toluene mineralization under sequential aerobic, denitrifying, and iron-reducing conditions in a closed batch system. TIC, total inorganic carbon.

out any lag period immediately after the start of the simulation. The degradation rate is highest at the beginning while oxygen is still present but decreases constantly over time. Once nitrate is depleted (after 8 days), the simulated $Fe(OH)_3$ concentration also starts to decrease. The simulation results in Fig. 4.5 show also that the total inorganic carbon concentration increases during the phase at which oxygen and nitrate act as electron acceptors. However, once iron reduction has started, the total inorganic carbon concentration starts to decrease again as the solution becomes (or, more precisely, would become) oversaturated with respect to siderite ($FeCO_3$), which therefore precipitates. Figure 4.5 also depicts pH changes during the three phases of the numerical experiment. The changes would even be more pronounced if calcite ($CaCO_3$) did not buffer the pH changes. The simulation results indicate therefore that even the (dissolved) calcium concentrations are ultimately affected by toluene oxidation.

MODELING FLOW AND PHYSICAL TRANSPORT

Nonreactive Single-Species Transport

The successful application of bioremediation techniques to contaminated groundwater is based on the availability of all essential ingredients required for the microbial activity to occur. In many groundwater systems, the rate of delivery of one or more of the reactants that take part in the transformation limits the progress of contaminant destruction. Clearly, groundwater flow and the resulting mixing caused by hydrodynamic dispersion play a key role for remediation success. Detailed understanding and quantification of the natural groundwater dynamics and/or the dynamics induced by a remediation scheme are essential for optimizing engineered schemes or predicting natural attenuation.

The macroscopic mass balance for the transport of a single, dissolved, nonreactive chemical species within a three-dimensional domain is described mathematically by the partial differential equation (10, 11, 67)

$$\frac{\partial C}{\partial t} = \frac{\partial}{\partial x_i}(D_{ij}\frac{\partial C}{\partial x_j}) - \frac{\partial}{\partial x_i}(v_i C) + \frac{q_s}{\theta}C_q \quad (32)$$

where C [ML^{-3}] is the aqueous concentration of the chemical species, v_i [LT^{-1}] is the pore water velocity in direction x_i [L], D_{ij} [L^2T^{-1}] is the hydrodynamic dispersion coefficient tensor (summation convention assumed), θ is the porosity of the porous medium, q_s [$L^3L^{-3}T^{-1}$] is the volumetric flux rate per unit volume of water representing external sources and sinks, and C_q [ML^{-3}] is the concentration of the species within this flux if q_s is positive (injection), otherwise $C_q = C$. In equation 32, the chemical species is subject to advective and dispersive transport by the flowing fluid.

The advection-dispersion equation results from averaging microscopic processes occurring at the pore scale within a representative elementary volume, leading to a continuum model at the macroscopic level (10). The advection term describes the transport of a dissolved species at the same mean velocity as the groundwater, which is the dominating physical process in most field-scale contamination problems within the saturated groundwater zone. The dispersion term represents two processes, mechanical dispersion and molecular diffusion. Mechanical dispersion results from the fluctuation of the (microscopic) streamlines in space with respect to the mean flow direction and inhomogeneous conductivities within the representative elementary volume. Molecular diffusion is caused by the random movement of the molecules in a fluid. It is usually negligible compared to mechanical dispersion (10). The (macroscopic) pore velocity v_i in equation 32 is derived from Darcy's law

$$v_i = -\frac{K_{ij}}{\theta}\frac{\partial h}{\partial x_j} \quad (33)$$

and the three-dimensional flow equation for saturated groundwater

$$\frac{\partial}{\partial x_i}\left(K_{ij}\frac{\partial h}{\partial x_j}\right) + q_s = S_s\frac{\partial h}{\partial t} \quad (34)$$

where K_{ij} is the hydraulic conductivity tensor and h [L] is the hydraulic head. Note that the off-diagonal entries of the hydraulic conductivity tensor become zero if the principal components are aligned with the x, y, and z axes of the flow domain. Analytical solutions for equations 32 to 34 exist only for relatively simple cases. Thus, for solving more complicated cases, e.g., involving heterogeneous aquifers, transient boundary conditions, etc., numerical techniques such as the finite difference and finite element methods (11, 34, 46, 62) are required. Groundwater flow models such as MODFLOW (40), HST3D (37), FEMWATER (65), and FEFLOW (20) that incorporate information on the hydrological and hydrogeological properties of a site will typically form the basis for subsequent contaminant transport simulations. However, in many cases, a proper groundwater flow model itself can already provide useful information, e.g., to estimate how fast the edge of a contamination front would migrate in a nonreactive case, i.e., if no biodegradation or sorption occurred.

Modeling packages such as PMPATH (16) allow predictions of the contaminant flow path and travel times of nonreactive contaminants.

The first step in building such a site-specific groundwater flow model is, based on a preliminary site characterization, the development of a conceptual hydrological and hydrogeological model. At this stage, all available geologic and hydrographic information is collated and analyzed. The conceptual model formulates the following qualitatively:

- the general groundwater flow direction;
- (natural) boundaries that might be used as boundaries in the numerical model, such as (subsurface) catchment boundaries and (dividing) streamlines;
- which stratigraphic layer(s) is more and which one is less or much less permeable, and which layer(s) is suitable to form a boundary in the numerical model; and
- the fluxes into and out of a chosen (model) domain and how to determine or estimate these fluxes quantitatively.

The so-constructed conceptual model might be translated into a simple numerical model, pointing to data gaps and thus assisting in the design of a refined characterization program and monitoring network. Details of this procedure can be found in many groundwater hydrology-specific textbooks such as those by Freeze and Cherry (28) or Fetter (26). Modeling texts such as those by Anderson and Woessner (2), Chiang and Kinzelbach (16), and Zheng and Bennett (68) are available also.

Reactive Single-Species Transport

The chemical species transported by groundwater as described by equation 32 will, in most cases, either interact with the aquifer material (e.g., sorption, ion exchange, or precipitation-dissolution) or react with other chemicals in the aqueous phase (e.g., acid-base reactions or redox reactions) or both. In a very general, unspecified form this can be expressed mathematically by including an additional reaction term, R_{chem}, in the above-mentioned transport equation, leading to

$$\frac{\partial C}{\partial t} = \frac{\partial}{\partial x_i}\left(D_{ij}\frac{\partial C}{\partial x_j}\right) - \frac{\partial}{\partial x_i}(v_i C) + \frac{q_s}{\theta}C_q + R_{\text{chem}} \qquad (35)$$

This reaction term is typically a complicated function of the concentrations of many other chemical species and/or of bacterial concentrations, for example. Limited by the availability of appropriate computational resources, these interactions between multiple groundwater and soil constituents were, until recently, neglected in most modeling applications. However, with the steady disappearance of this constraint, models of increasing complexity have been developed.

COUPLED PHYSICAL TRANSPORT AND REACTIVE PROCESSES

We now consider the case where physical transport and reactive processes occur simultaneously. To solve this type of problem, a range of numerical schemes exists (e.g., see reference 56). We focus here, however, on only one particular method, the split-operator technique (6–8, 33, 66), which is (i) simple to understand, (ii) relatively easy to implement on parallel computers, and (iii) with few exceptions (e.g., OS3D/GIMRT software from Pacific Northwest National Laboratory, Richland, Wash.) has become the standard method for solving such combined physicochemical problems. The operator-splitting technique involves separating the processes (e.g., flow, transport of individual chemical components or species, chemical reactions, and microbial activity) within the numerical model and solving each submodel independently. Different implementations of this method exist, resulting in different degrees of accuracy and computational burden. In the most simple and commonly applied variation, equation 32 is initially solved separately for each transported chemical for each time step of length Δt before, in a second step, the concentration changes due to chemical reactions during Δt are determined. The latter computation is carried out for each grid cell (in a spatially discretized

domain) independently from other grid cells, thereby simplifying the computational burden significantly compared with that of the fully coupled case. The rates at which the reactions proceed in relation to the velocity at which the chemicals are transported provide the criteria for choosing an appropriate solution technique to accurately describe the reactive processes. Under the assumption that all reactive processes proceed rapidly in comparison to groundwater flow and transport, known as the local equilibrium assumption, equilibrium thermodynamics can be used to compute the concentration changes. Note that within this (equilibration) step, each grid cell is treated as a closed system. That is, the total concentration of each chemical component, consisting of the sum of aqueous, sorbed, precipitated and gas-phase concentrations, does not change, although the distribution within these phases and the concentration of (complexed) species will vary. Batch-type geochemical equilibrium packages such as PHREEQE/PHREEQC (43, 44) or MINTEQA2 (1) can be used for this step. Engesgaard and Kipp (23) and Walter et al. (61) presented examples of models employing this technique. More recently, the split-operator technique has been applied to model sets of multiple, exclusively kinetically reacting species (e.g., see reference 18) or for problems where both equilibrium and kinetic reactions occur. The PHREEQC-2 model (45), which we have already used for the batch-type examples, can be used for a modeling approach of the latter class. Coupled to a transport model via operator splitting, it is capable of determining the reaction term R_{chem} within equation 35 for a wide variety of sets of mixed equilibrium and kinetic reactions (15, 49, 50; also PHAST [http://www.brr.cr.usgs.gov/projects/GWC_coupled/phast/] from the U.S. Geological Survey). Below, we will explore some of the major aspects and typical applications related to bioremediation.

MODELING OF NATURAL ATTENUATION PROCESSES

More than in other areas of bioremediation, numerical modeling is applied to assist the assessment of site-specific risks when natural attenuation is the preferred remediation option. In many cases it can be expected that the dissolution from free product, i.e., non-aqueous-phase liquids (NAPLs), in the vicinity of the saturated groundwater zone will provide a long-term contamination source for the groundwater, perhaps lasting decades or even hundreds of years. Under most circumstances that involve NAPL dissolution, groundwater contaminant plumes of a more or less stable length will form during a relatively short timescale (30). Stable plumes occur under conditions where the total mass dissolved from the free product (per unit of time) equals the rate of total contaminant mass destruction by biodegradation. In the case of oxidizable organic compounds such as petroleum hydrocarbons (or landfill leachates), typically one or more electron acceptors will be consumed so that distinct redox zones form downstream of the contaminant source (5, 12). They are the result of the sequential use of electron acceptors, with the most reduced chemical environment being the plume center in proximity of the source region. The key factors that are largely responsible for the length of steady-state plumes are:

- groundwater flow velocity,
- rate of organic compound dissolution from free product or NAPL in the source zone,
- oxidation capacity provided by the background or uncontaminated water, and
- mixing of electron acceptors through transverse hydrodynamic dispersion.

In the following section, we will discuss some of the important modeling aspects of these governing factors.

Modeling the Contamination Source

In most cases where numerical modeling is applied to field-scale contamination problems, the extent and the location of the source of the contamination are not well characterized. In order to reduce the uncertainty associated with the lack of detailed information, the migration of the contaminant might be simulated as a multiphase problem involving water, air, and

oil (25). However, in many instances, in particular when the oil phase is denser than water, the source location and extension must be largely guessed. With the known or estimated location of the contamination source, the (simultaneous) mass transfer of multiple organic compounds from the NAPL phase to the water phase and the (dissolved) concentrations of the organic compounds can be approximated. For the n_{org} organic compounds that are present in the NAPL phase, nonequilibrium mass transfer, r_{dis}, from a NAPL pool is expressed as

$$\frac{\partial C_i^{\text{dis}}}{\partial t} = \varpi_i \left(C_i^{\text{sat, mc}} - C_i \right) \qquad (36)$$

where ϖ_i [T^{-1}] is a rate transfer coefficient approaching infinity for equilibrium dissolution, C_i [ML^{-3}] is the aqueous species concentration of the ith organic compound, and $C_i^{\text{sat, mc}}$ [ML^{-3}] is the multicomponent solubility of the ith organic compound. The multicomponent solubility is calculated according to Raoult's law:

$$C_i^{\text{sat, mc}} = C_i^{\text{sat}} \gamma_i m_i \qquad (37)$$

where C_i^{sat} [ML^{-3}] is the single-species solubility, γ_i is the activity coefficient of the ith organic compound (typically for simplicity assumed to be unity), and m_i is the mole fraction of the ith organic compound. The mole fraction is defined as

$$m_i = \frac{n_i}{n_{\text{tot}}} \qquad (38)$$

where n_i is the molar concentration of compound i in the NAPL and n_{tot} is the total molar concentration of all organic compounds in the NAPL. From equations 36 to 38 it becomes clear that the near-source concentrations might change with time due to the temporal change in the molar fraction. When the dissolution process is kinetically controlled, concentrations will also depend on the groundwater flow velocity.

As a first example for a coupled transport and reaction simulation, we look at a simple, one-dimensional transport problem where uncontaminated, anaerobic, sulfate-rich ground water is passing a 4-m-long aquifer zone (located between 5 and 9 m from the left influent boundary) contaminated with residual NAPL blobs. The groundwater flow rate is constant, i.e., pore velocity of 0.75 m day^{-1} (case 6; initial concentrations are given in Table 4.4). We assume that the residual NAPL consists only of the four BTEX compounds as, in practice, they are the most soluble gasoline constituents. As before, we assume that sulfate and dissolved BTEX compounds act as electron acceptors and electron donors, respectively. Only the activity of SRB attached to the aquifer matrix is simulated; i.e., any detachment-attachment and transport processes of SRB are considered negligible. As the simulation results for this simple system show (Fig. 4.6), there is an increase of BTEX concentra-

TABLE 4.4 Initial concentrations of NAPLs, aqueous components, and microbes in the uncontaminated aquifer (cases 6 and 7)

Component or bacteria	Concn (mol/liter)
Inorganic aqueous components[a]	
O(0)[b]	0.0
S(VI)	2.50×10^{-3}
S(−II)	0.0
Fe(II)	5.78×10^{-5}
Fe(III)	1.60×10^{-12}
C(IV)	7.95×10^{-3}
Ca	5.00×10^{-3}
Mg	5.66×10^{-4}
Na	5.24×10^{-3}
K	2.59×10^{-4}
Cl	6.44×10^{-3}
Organic compound or bacteria	
Non-NAPL	
Benzene	0.0
Toluene	0.0
Ethylbenzene	0.0
Xylene	0.0
NAPL	
Benzene	2.0
Toluene	5.0
Ethylbenzene	2.0
Xylene	1.0
SRB	1.0×10^{-8}

[a] pH, 6.57; pe (measure of electron activity in aqueous solution), −2.08.
[b] Values in parentheses indicate valence state.

tions within the NAPL-containing zone, with the maximum concentrations varying significantly due to the different mole fractions of the compounds in the NAPL mix and due to their different (single-component) aqueous solubilities (C^{sat}). The BTEX compounds are undergoing biodegradation within and downstream of the source zone as long as sulfate is available, so that toluene, ethylbenzene, and xylene are completely removed, but not benzene. Since no other degradation processes that involve less favorable electron acceptors such as iron reduction or methanogenesis are modeled here, no further contaminant destruction occurs once sulfate is depleted.

Role of Dispersive Mixing

Under such circumstances, transverse dispersion becomes the mechanism that controls the fate of the remaining, undegraded portion of the

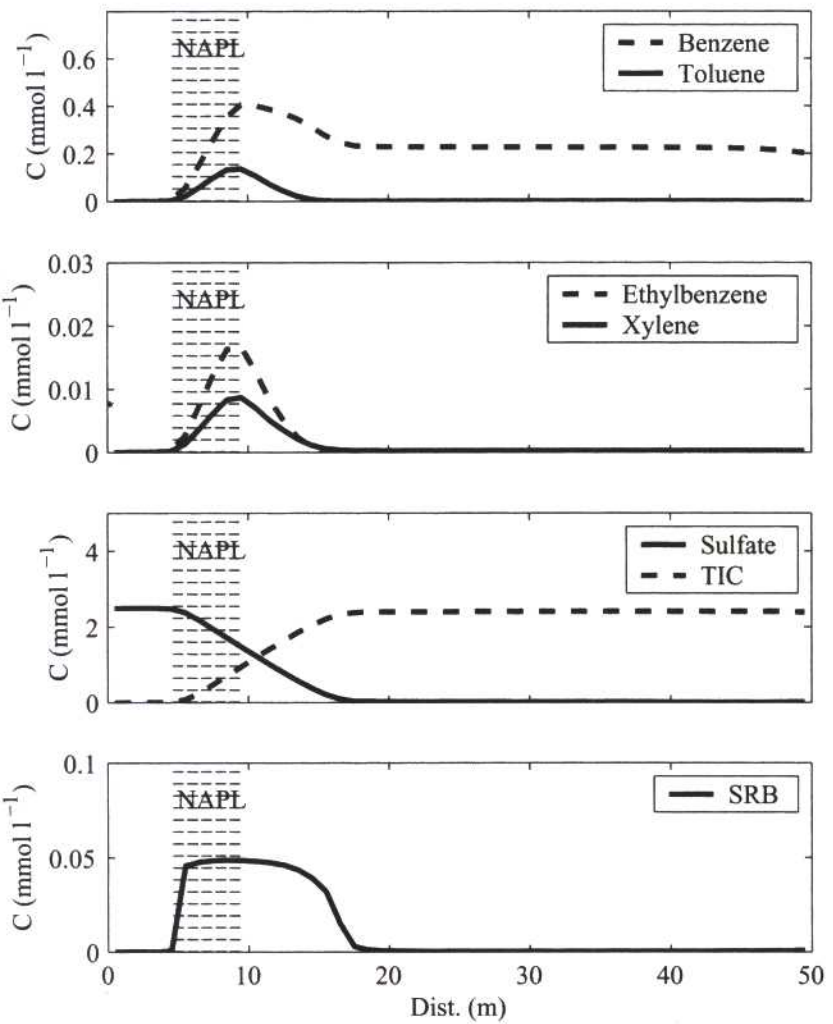

FIGURE 4.6 Simulation of BTEX compound dissolution, transport, and mineralization under sulfate-reducing conditions in a one-dimensional domain. The NAPL source zone is located between 5 and 9 m from the influent end (left). TIC, total inorganic carbon.

mass released from the NAPL source. Of course, the one-dimensional model is unable to capture this, at least in a direct manner. Thus, a multidimensional transport simulation is necessary. Using the same "chemical" system, i.e., the same initial or inflow concentrations (Table 4.4) and parameters, and a groundwater flow rate similar to that of the previous case, the next case (case 7), a two-dimensional simulation, demonstrates the effect of (horizontal) transverse dispersion (Fig. 4.7). A microbial "fringe" develops downstream of the source zone at locations where degradable organic substances and electron acceptor are present simultaneously. A major problem in terms of modeling such cases arises from the fact that the apparent transverse dispersivity of nonreacting solutes does not necessarily provide a good estimate for bioreactive transport, as was pointed out, e.g., by Cirpka et al. (17). Using a streamline-oriented grid, they investigated the two-dimensional physical transport in a heterogeneous aquifer coupled to biodegradation reactions of a single-substrate, single-electron-acceptor system. They demonstrated that employing a Fickian macrodispersion model and using transverse dispersivities (deduced from the second spatial concentration moment transverse to flow direction) will significantly overestimate local-scale mixing and thus biodegradation rates. When physical transport is dominated by advection, i.e., hydrodynamic dispersion is small compared to advective

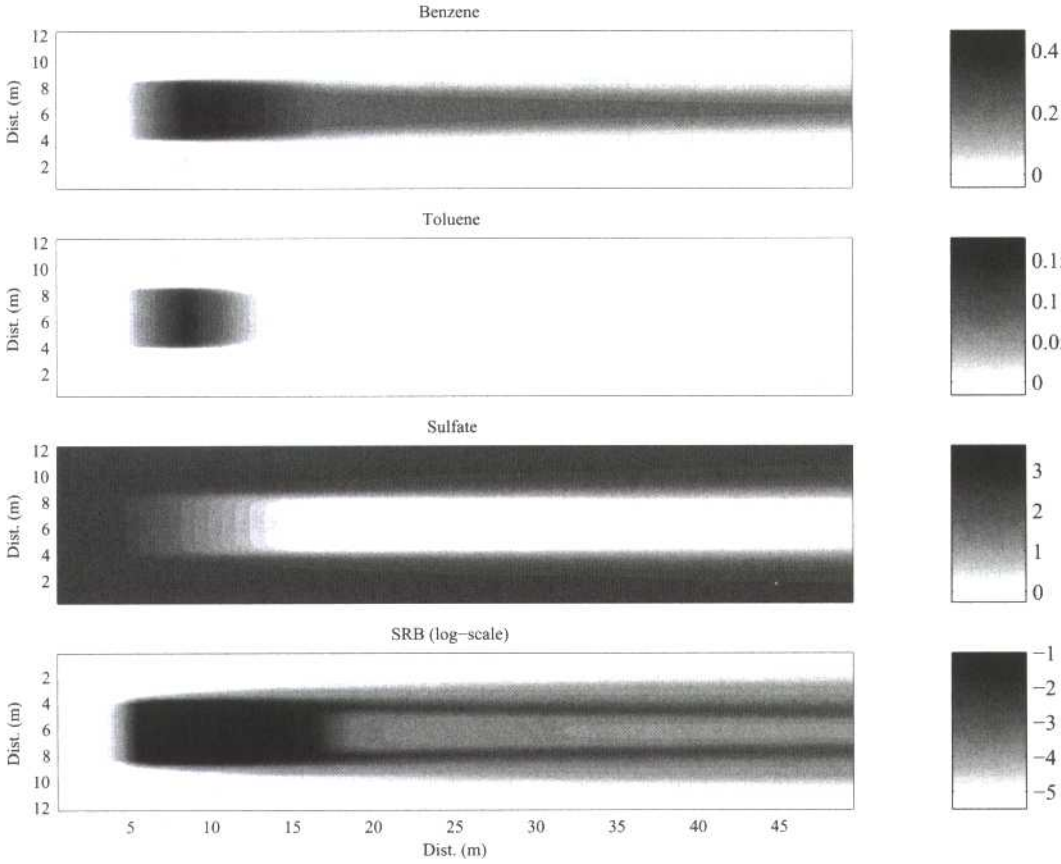

FIGURE 4.7 Simulation of BTEX compound dissolution, transport, and mineralization under sulfate-reducing conditions in a two-dimensional domain. The NAPL source zone is located between 5 and 9 m from the influent end (left) and has a width of 6 m. Dist., distance.

transport, these fringes might be very thin, resulting in steep chemical gradients. Resolution of the physical transport mechanisms in local regions without introducing large numerical errors remains a challenging and computationally expensive task, in particular for heterogeneous aquifers.

FIELD-SCALE APPLICATION

A numerical study was carried out for a BTEX-contaminated field site for which a wealth of detailed information of hydrochemical and microbial parameters has been intensively recorded. The field site is located in Perth, Western Australia (e.g., see reference 19), where toluene, ethylbenzene, and xylenes are mineralized under exclusively sulfate-reducing conditions. The modeling study is described in full detail elsewhere (50). Vertical concentration profiles obtained from multilevel sampling devices showed only limited vertical spreading of the long, thin plumes, indicating that the porous medium is fairly homogeneous and that transverse dispersion is rather small. As part of a more detailed modeling study, the flow, transport, and mixing processes and how they affect the site-specific degradation behavior were initially studied in a vertical cross-sectional model along the (flow) path of the contaminants, reported here as case 8. The specific scope of the numerical study was to further understand the site-specific role of the additional transverse dispersion, caused by the transient flow field, on reactive processes and, in particular, to determine whether this mechanism is likely to enhance natural attenuation significantly. In order to quantify the effect of the transient flow field, comparisons are made with transport simulations based on a steady-state condition.

Nonreactive-Single-Species Transport

The schematic vertical cross-sectional model was developed such that it approximately reproduces the hydro(geo)logical properties of the field site (19, 27, 54, 57). For example, recharge and inflow at the model upstream boundary were chosen so that the model would schematically represent the typical Perth climate of a 5-month rainy period (recharge of 1.5 mm day^{-1}) and a 7-month dry period without recharge. With a hydraulic conductivity of 22 m day^{-1}, the transient-flow model of the unconfined aquifer does indeed mimic the observed annual pattern of the piezometric heads. Water table fluctuations of almost 2 m occur at the influent boundary in response to the seasonally varying recharge. In the steady-state model, which was used for comparison, the recharge and boundary inflows were averaged over one annual cycle. For both the transient and the steady-state simulations, the groundwater flow field is characterized by increasing flow velocities towards the effluent boundary. This effect can be attributed to the nonsloping aquifer bottom, which, together with the falling water table (in flow direction), leads to a notable reduction of the effective thickness of the aquifer and consequently higher flow velocities. The computation of the first and second spatial moments can be used to indicate the location of the plume center and to quantify the spreading that the plume has undergone. The plots in Fig. 4.8 show the computed spatial moments along the flow direction. Snapshots for the transient plume behavior from different stages during the annual cycle are plotted in comparison with the corresponding results from the steady-state model. It can be seen that independently of dispersion and sorption the vertically integrated mass decreases along the flow path despite the absence of degradation reactions. Of course, in reality no mass has been destroyed. The example shows, rather, that the interpretation of measured concentrations, even when integrated in one or two spatial directions, can be misleading if no flux weighting is applied. In the absence of flux weighting, a proper conservation of mass is not warranted and the disappearance of the

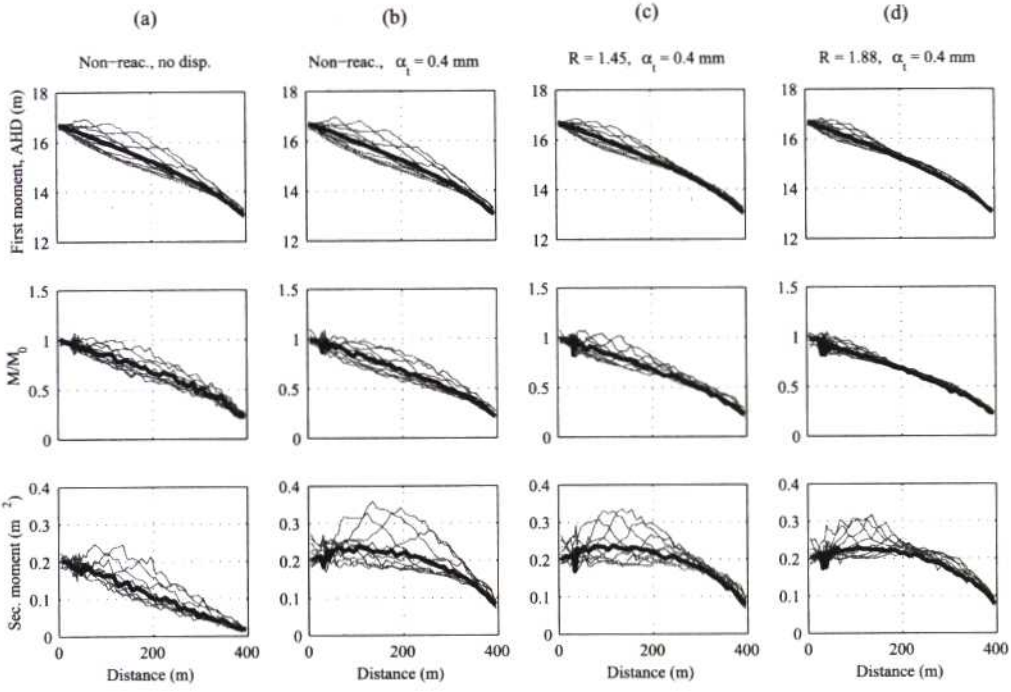

FIGURE 4.8 First-moment, vertically integrated mass and second moment for advective, nonreactive transport (a), advective, dispersive, nonreactive transport (b), and advective, dispersive transport with linear equilibrium sorption (retardation factors R of 1.45 and 1.88, respectively) (c and d). The solution for steady-state flow (thick lines) and solutions from the transient simulations (thin lines) are indicated. Reprinted from reference 50 with permission from Elsevier.

vertically integrated concentrations could be interpreted as biodegradation.

The effect of sorption reactions on the discussed plume characteristics was investigated by comparing "no-sorption" simulations with two scenarios that included linear equilibrium sorption reactions. In the first scenario, the sorption corresponds to a retardation factor of $R = 1.45$ and, in the second, to $R = 1.88$. The simulation results shown in Fig. 4.8 demonstrate that the inclusion of the sorption reactions exceeds a "buffering" effect on the vertical movement of the plume that results from seasonal hydraulic changes. This is indicated by the smaller variability of the computed first spatial moment (vertical position of plume center) and the computed second spatial moment (plume spreading). The results also show that for the transverse dispersivity used in these simulations (0.4 mm), the accelerating flow has a converging effect for the plume that is even stronger than the spreading caused by hydrodynamic dispersion. More details are given elsewhere (50).

Reactive Multicomponent Transport

Based on the previous simulations, in which degradation reactions were ignored, the influence of the transient flow field on reactive processes was studied in a second step. As discussed earlier in this chapter, biodegradation of oxidizable contaminants (in this case, BTEX compounds) might occur mainly at contaminant plume fringes where organic substrates and electron acceptors (in the present case sulfate) are simultaneously available. Thus, it might be intuitively expected that the vertical movement of the plume caused by the seasonal water table fluctuations would facilitate increased mixing of

reactants and that in response the rates of total mass removal by biodegradation would increase. This increased mixing of reactants might be expected when electron donor(s) and electron acceptor(s) have different sorption characteristics. The reactive multicomponent transport model PHT3D (49) was used to investigate the magnitude of this effect by comparing the results from reactive transport simulations that use a transient flow field with the corresponding results from simulations based on a steady-state flow field.

Previous studies (19, 48) identified sulfate reduction as the dominant mechanism for the attenuation of BTEX compounds. Oxygen was observed only in low concentrations in the proximity of the water table during times of recharge. There it is consumed rapidly, either directly by organic matter or by groundwater constituents and/or minerals that have been reduced previously. Nitrate was generally not found in this portion of the aquifer. The water composition used for the numerical study, which was assumed to be representative for the uncontaminated portion of the aquifer, was based on a water sample taken upstream of the contaminated area. The recharge water was assumed to have an identical composition, except that the solution had been equilibrated with an additional 3.2 mg of oxygen liter^{-1}. Two minerals (pyrite and siderite) that had been identified as reaction products in a soil core taken within the contaminated zone (48) were also included in the simulation. SRB and toluene (other organic compounds were excluded) were treated as kinetic species for which rate expressions were formulated on the basis of the concepts discussed earlier in this chapter.

Contamination Source

The investigation of core material from the contamination source zone showed that residual NAPLs were distributed over a 1- to 1.5-m-thick zone below the water table (19). The measurements of dissolved concentrations from a nearby multilevel sampling device indicated that the location and vertical extent of the zone from which elevated concentrations of BTEX compounds dissolve would largely follow the

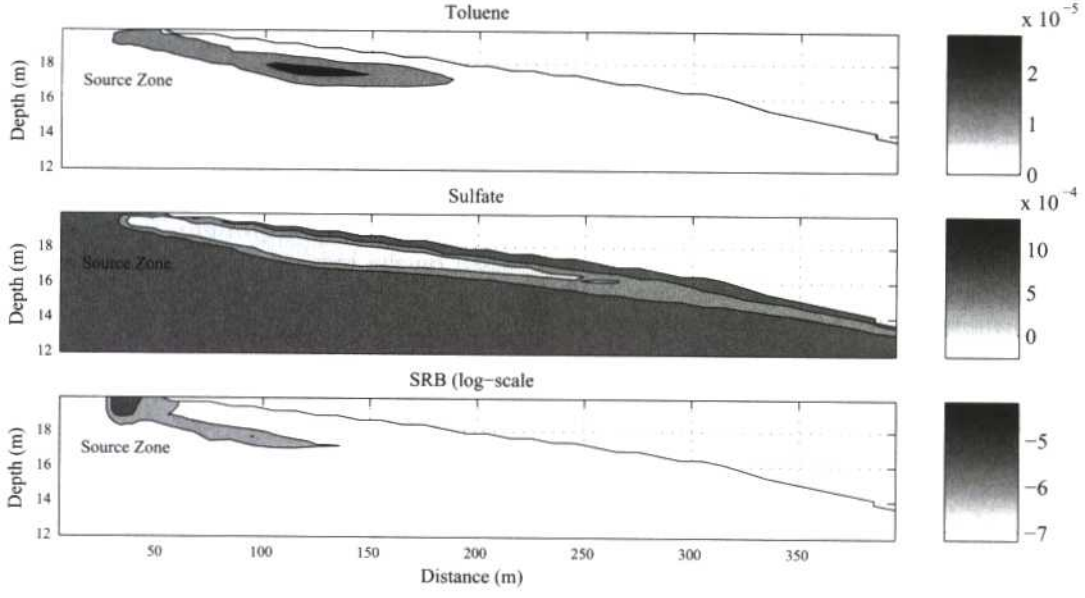

FIGURE 4.9 Contour plots for toluene, sulfate, and SRB for a snapshot from the transient simulations (concentrations are given in moles per liter) (after the work of Prommer et al. [50]).

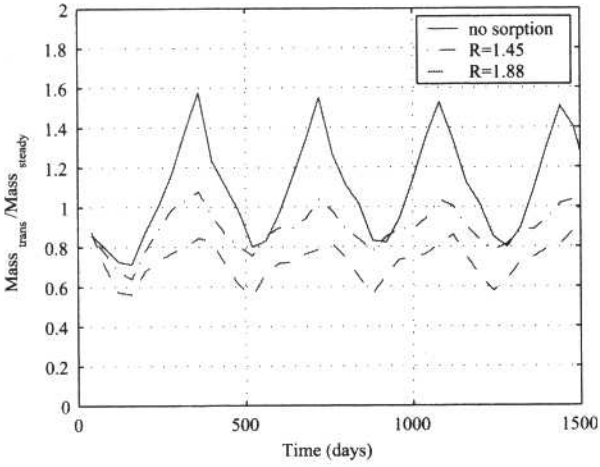

FIGURE 4.10 Simulated total mass (concentrations integrated over the model domain) of toluene during the transient (trans) simulations. Reprinted from reference 50 with permission from Elsevier.

movement of the water table. However, the lower portion of this NAPL dissolution zone appeared to move somewhat more slowly than the water table itself at times of a rising water table. The latter effect was not considered in the numerical model study. Instead, the vertically moving NAPL dissolution zone was modeled to occur from a defined, constant thickness below the moving water table.

Steady-State versus Transient Simulations

The reactive transport simulations reproduce the observed thin toluene plumes and their approximate length, which is limited by the mass removal through biodegradation. The results show the observed limited vertical extent of the sulfate-depleted zone, confirming that the transverse dispersivity at this site is small. The simulations illustrate that the activity of the bacteria, i.e., their highest concentrations, occurs mainly in the vicinity of the contamination source and, further downstream, at the plume fringes where the presence of sulfate and toluene overlaps. The seasonally changing flow and, in particular, the "moving" contaminant source lead to pronounced seasonal variability of contaminant dissolution and its flow path and biogeochemical reaction rates. A snapshot from those transient simulations is shown in Fig. 4.9 for toluene, sulfate, and SRB concentrations. The local (integrated) mass of dissolved toluene in the model varies between 60 and 160% of the corresponding steady-state mass, as can be seen in Fig. 4.10. The plot also identifies the effect of toluene sorption, which reduces the seasonal variability of the total mass. It can be seen that on average, the total mass decreases with increasing

TABLE 4.5 Initial concentrations of aqueous components, minerals, and microbes in the uncontaminated aquifer used in the field-scale natural attenuation simulation (case 8)

Component or bacteria	Concn (mol/liter)
Aqueous components[a]	
O(0)[b]	0.0
S(VI)	7.84×10^{-4}
S(−II)	0.0
Fe(II)	6.65×10^{-5}
Fe(III)	2.14×10^{-12}
C(IV)	7.95×10^{-3}
Ca	8.41×10^{-4}
Cl	6.44×10^{-3}
Mg	5.66×10^{-4}
Na	5.24×10^{-3}
K	2.59×10^{-4}
Minerals or bacteria	
Pyrite	0
Siderite	0
SRB	1.00×10^{-8}

[a] pH, 5.06; pe, 1.21.
[b] Values in parentheses indicate valence state.

sorption. This shows that the modeled toluene sorption indeed causes a notable chromatographic effect by slowing down the vertical movement of the toluene plume relative to the somewhat faster vertical movement of the sulfate-depleted zone. The effect leads to enhanced mixing between toluene and sulfate-containing water. If toluene sorption is excluded, the overall influence of the seasonally changing flow on mass removal by biodegradation remains rather small.

MODELING OF ENHANCED BIOREMEDIATION

As stated above, very often the supply of electron acceptors is the critical factor for natural attenuation, i.e., the length of a plume. In such cases, the addition of electron acceptors, in many cases together with other potentially growth-limiting substances, might be used as a means to enhance and accelerate naturally occurring degradation processes. However, the choice among electron acceptors is not necessarily straightforward, as discussed, e.g., by Kinzelbach et al. (36). Oxygen has the advantage of having the highest molecular energy yield. Unfortunately, its low solubility in water is a limiting factor for the transfer of oxidation capacity to an aquifer. Sulfate has a higher solubility but is accompanied by a sometimes undesired hydrogen sulfide production. Furthermore, sulfate reduction might not be able to degrade efficiently more recalcitrant oxidizable organic substances. In terms of modeling enhanced remediation processes, the two major challenges are:

- choice of reactive processes to be included in a simulation, and
- accurate representation of the local-scale mixing processes that mix the injected water with the contaminated water.

TABLE 4.6 Initial concentrations of aqueous components, minerals, and bacteria of the initially contaminated aquifer and of the oxygenated water that is injected to enhance remediation

Aqueous component, mineral, or bacterial group	Concn (mol/liter) in case 9a (primary reactions only)		Concn (mol/liter) in case 9b (primary and secondary reactions)[a]	
	$C_{initial}$	C_{inflow}	$C_{initial}$	C_{inflow}
Toluene	3×10^{-5}	0	3×10^{-5}	0
N(5)	—[b]	—	0.0	5.0×10^{-4}
N(3)	—	—	0.0	0.0
N(0)	—	—	5.0×10^{-4}	0.0
N(−3)	—	—	1.10×10^{-6}	0.0
O(0)	0.0	6.32×10^{-4}	0.0	6.32×10^{-4}
S(VI)	—	—	5.26×10^{-4}	5.0×10^{-4}
S(-II)	—	—	5.07×10^{-11}	0.0
Fe(II)	—	—	2.58×10^{-6}	0.0
Fe(III)	—	—	3.48×10^{-13}	1.79×10^{-12}
C(IV)	—	—	3.19×10^{-3}	1.70×10^{-4}
Ca	—	—	1.90×10^{-3}	1.43×10^{-3}
Na	—	—	4.35×10^{-4}	4.35×10^{-4}
Cl	—	—	2.82×10^{-4}	2.82×10^{-4}
Pyrite	—	—	8.00×10^{-3}	—
Goethite	—	—	0	—
Aerobes[c]	1.0×10^{-8}	—	1.0×10^{-8}	—

[a] pH, 7.32; pe (measure of electron activity in an aqueous solution), −3.16.
[b] —, not considered in simulation.
[c] Concentrations given in number of organisms per milliliter.

In order to illustrate the first point, i.e., the importance of choosing the correct conceptual model, we set up a simple example of enhanced remediation via pulsed injection of oxygenated water into an anaerobic, heterogeneous, initially toluene-contaminated aquifer (case 9) and compare the results for two sets of reactions. In the first case, we consider only the (primary) biodegradation reaction, here the degradation of toluene under aerobic conditions. To model this, the reactions include only toluene, oxygen, and aerobic degraders. In contrast, in the second modeling approach, we additionally describe the composition of the groundwater and of major minerals in more detail and thus define the oxidation state of the aquifer (Tables 4.5 and 4.6). In this example, we include the presence of reduced aqueous species and of pyrite (FeS_2). As a consequence, oxygen that is injected to enhance the breakdown of the organic contaminants is partially diverted to other oxygen-consuming processes, i.e., the reoxidation of pyrite and of ammonia. As shown, e.g., by the biogeochemical modeling exercise of Thullner and Schäfer (58), such a diversion to minerals might consume a large fraction of the oxidation capacity that is added by the remediation scheme. In this case, it was estimated that only 2% of the oxygen mass added was consumed by the contaminants, whereas 56% of the oxygen injected was diverted to pyrite oxidation. Figure 4.11 shows a comparison of these two reaction

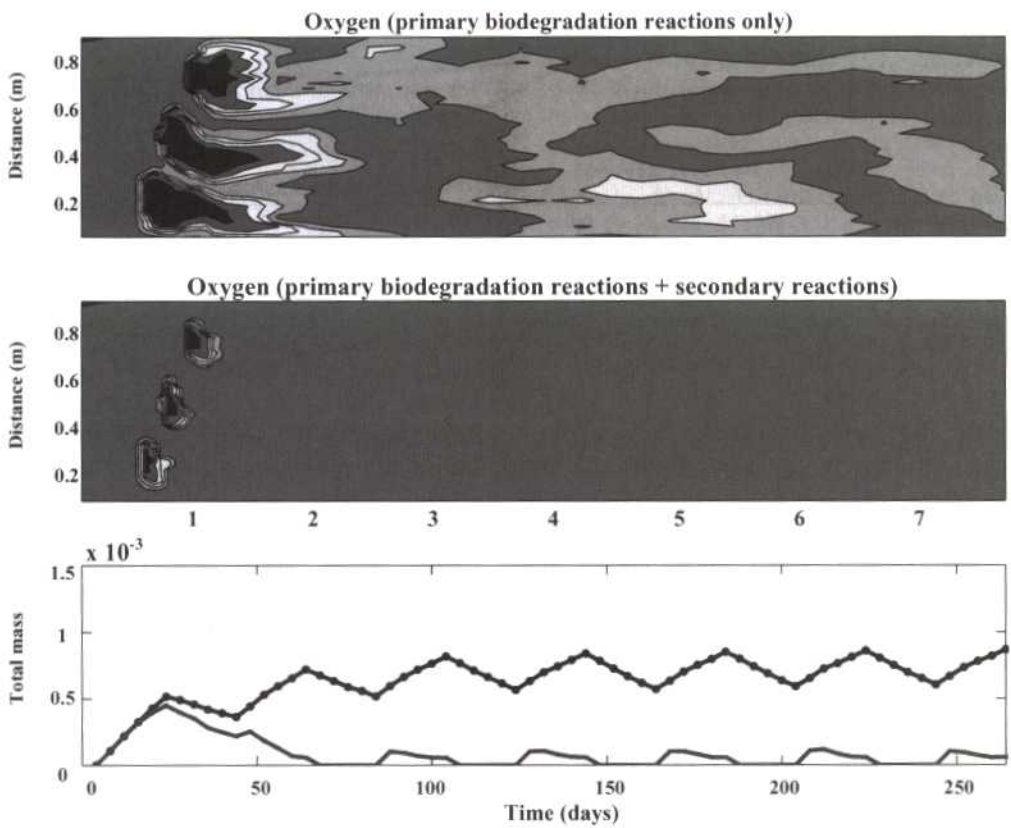

FIGURE 4.11 Simulation of enhanced remediation of toluene by injection of oxygenated water, showing oxygen concentration distribution when primary reactions only (above) and primary and secondary oxygen-consuming reactions (middle) are considered.

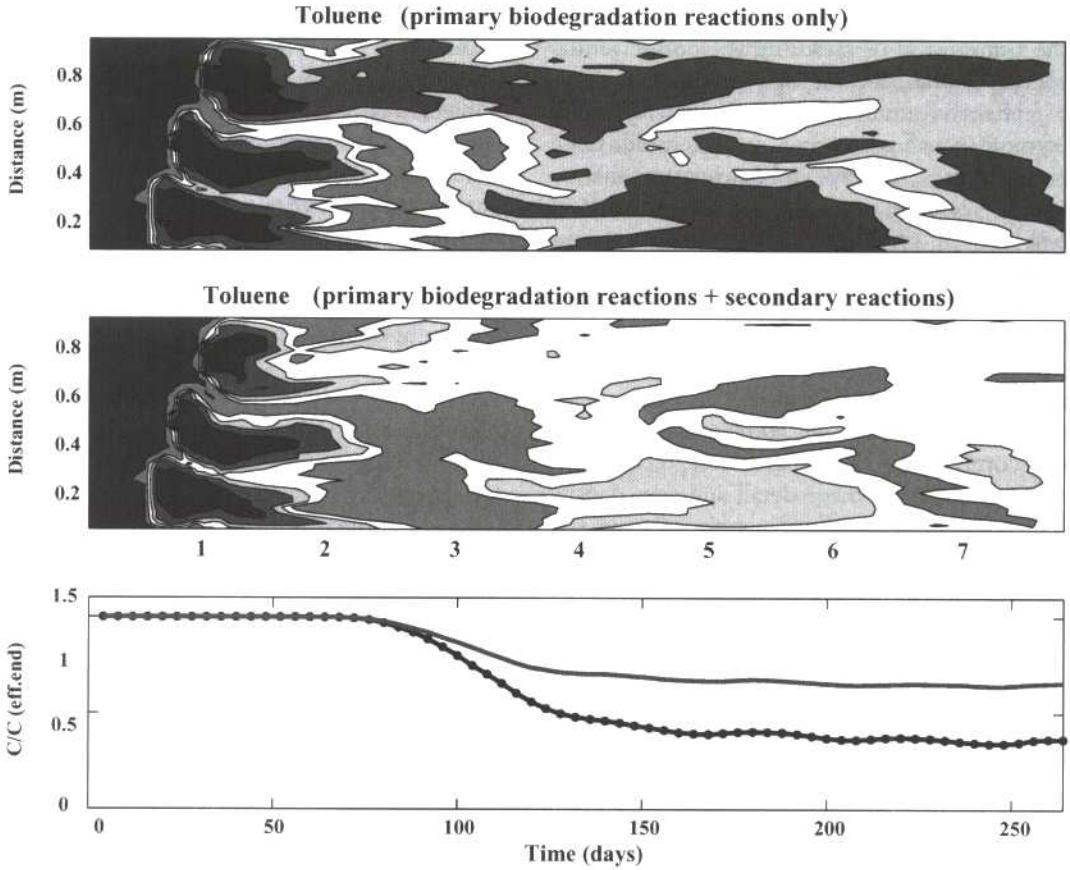

FIGURE 4.12 Simulation of enhanced remediation of toluene by injection of oxygenated water, showing toluene concentration distribution when only primary reactions (top) and both primary and secondary reactions (middle) are considered.

models. The figure shows the oxygen concentration 200 days after the beginning of the remediation and the temporal development of the integrated oxygen concentration, i.e., the total mass of oxygen in the model domain versus time. The corresponding toluene concentrations are shown in Fig. 4.12, where the large difference in the amount of toluene mass that is degraded within the model boundaries is apparent. Confirming the findings of our simplified case, Eckert and Appelo (21) reported the results from a BTEX-contaminated site in Germany where KNO_3 injection was used for enhanced remediation. The associated geochemical transport model study also highlights that a significant portion of the injected oxidation capacity was consumed by sulfide minerals. The fraction of the injected oxidants that is lost to untargeted reactions depends of course on the reaction kinetics (rates) of the competing reactions. Some knowledge regarding the reactivity of reduced sediments has been developed in studies such as that presented by Hartog et al. (31, 32), but it is far from complete.

CONCLUDING REMARKS

In this chapter, we have introduced some of the key concepts that might play a role for the use of numerical modeling in the context of bioremediation. Emphasis was put on reviewing how the underlying chemical and physical

processes are translated into a coupled framework that simultaneously deals with both aspects. The theory and examples that we discussed here were confined to problems in the water-saturated zone, where biodegradation modeling probably finds its major applications. For simplicity, we have also focused the discussions on one particular contaminant class (oxidizable organic compounds). However, topics where modeling of transport in combination with microbially mediated reactions has also been applied include, for example:

- biodegradation modeling in the unsaturated zone,
- biodegradation of NAPLs in combination with multiphase transport,
- in situ metal precipitation by injection of nontoxic degradable organic substances, and
- biodegradation of chlorinated hydrocarbons.

All of these problems have in common the fact that they integrate interdisciplinary knowledge developed by microbiologists, geochemists, hydrogeologists, mathematicians, and engineers. Of course, a key factor for the successful development and application of such biodegradation models is always to find the necessary balance of process detail for each of the physical, chemical, or microbial processes that are considered. Therefore, it is important to have toolbox-like models at hand, so that additional process detail can be quickly incorporated (or redundant details can be eliminated) and to allow a quick adjustment of simulation tools to evolutionary changes of conceptual models. In all cases, the right balance between the complexity of models and the data that are available to underpin its use must also be found.

REFERENCES

1. **Allison, J. D., D. S. Brown, and K. J. Novo-Gradac.** 1991. *MINTEQA2/PRODEF2, A Geochemical Assessment Model for Environmental Systems: Version 3.0 User's Manual.* Technical report EPA/600/3–91/021. U.S. Environmental Protection Agency, Athens, Ga.
2. **Anderson, M. P., and W. W. Woessner.** 1992. *Applied Groundwater Modeling Simulation of Flow and Advective Transport.* Academic Press, San Diego, Calif.
3. **Bae, W., and B. E. Rittmann.** 1996. A structured model of dual-limitation kinetics. *Biotechnol. Bioeng.* **49:**683–689.
4. **Bae, W., and B. E. Rittmann.** 1996. Responses of intracellular cofactors to single and dual limitation. *Biotechnol. Bioeng.* **49:**690–699.
5. **Baedecker, M. J., I. M. Cozarelli, D. I. Siegel, P. C. Bennett, and R. P. Eganhouse.** 1993. Crude oil in a shallow sand and gravel aquifer. 3. Biogeochemical reactions and mass balance modeling. *Appl. Geochem.* **8:**569–586.
6. **Barry, D. A., K. Bajracharya, and C. T. Miller.** 1996. Alternative split-operator approach for solving chemical reaction/groundwater transport models. *Adv. Water Resouces* **19:**261–275.
7. **Barry, D. A., C. T. Miller, and P. J. Culligan-Hensley.** 1996. Temporal discretisation errors in non-iterative split-operator approaches to solving chemical reaction/groundwater transport models. *J. Contam. Hydrol.* **22:**1–17.
8. **Barry, D. A., C. T. Miller, P. J. Culligan, and K. Bajracharya.** 1997. Analysis of split operator methods for nonlinear and multispecies groundwater chemical transport models. *Math. Comput. Sim.* **43:**331–341.
9. **Barry, D. A., H. Prommer, C. T. Miller, P. Engesgaard, and C. Zheng.** 2002. Modelling the fate of oxidisable organic contaminants in groundwater. *Adv. Water Resources* **25:**945–983.
10. **Bear, J.** 1972. *Dynamics of Fluids in Porous Media.* Dover Publications Inc., New York, N. Y.
11. **Bear, J., and A. Verruijt.** 1987. *Modeling Groundwater Flow and Pollution.* D. Reidel Publishing Co., Dordrecht, The Netherlands.
12. **Bjerg, P. L., K. Rügge, J. K. Pedersen, and T. H. Christensen.** 1995. Distribution of redox sensitive groundwater quality parameters downgradient of a landfill (Grindsted, Denmark). *Environ. Sci. Technol.* **29:**1387–1394.
13. **Borden, R. C., P. B. Bedient, M. D. Lee, C. H. Ward, and J. T. Wilson.** 1986. Transport of dissolved hydrocarbons influenced by oxygen-limited biodegradation. 2. Field application. *Water Resource Res.* **22:**1973–1982.
14. **Brock, T. D., M. T. Madigan, J. M. Martinko, and J. Parker.** 1994. *Biology of Microorganisms.* Prentice-Hall, Englewood Cliffs, N.J.
15. **Brun, A., and P. Engesgaard.** 2002. Modelling of transport and biogeochemical processes in pollution plumes: literature review and model development. *J. Hydrol.* **256:**211–227.

16. **Chiang, W.-H., and W. Kinzelbach.** 2000. *3D Groundwater Modeling with PMWIN: A Simulation System for Modeling Groundwater Flow and Pollution.* Springer-Verlag, Berlin, Germany.
17. **Cirpka, O. A., E. O. Frind, and R. Helmig.** 1999. Numerical simulation of biodegradation controlled by transverse mixing. *J. Contam. Hydrol.* **40:**159–182.
18. **Clement, T. P.** 1997. *RT3D—A Modular Computer Code for Simulating Reactive Multi-Species Transport in 3-Dimensional Groundwater Systems.* PNNL-SA-28967. Battelle Pacific Northwest National Laboratory, Richland, Wash.
19. **Davis, G. B., C. Barber, T. R. Power, J. Thierrin, B. M. Patterson, J. L. Rayner, and W. Qinglong.** 1999. The variability and intrinsic remediation of a BTEX plume in anaerobic sulfate-rich groundwater. *J. Contam. Hydrol.* **36:** 265–290.
20. **Diersch, H.-J. G.** 1997. *Interactive, Graphics-Based Finite-Element Simulation System FEFLOW for Modelling Groundwater Flow. Contaminant Mass and Heat Transport Processes.* User's manual version 4.6. WASY. Institute for Water Resources Planning and System Research Ltd., Berlin, Germany.
21. **Eckert, P., and C. A. J. Appelo.** 2002. Hydrogeochemical modeling of enhanced benzene, toluene, ethylbenzene, xylene (BTEX) remediation with nitrate. *Water Resource Res.* **38:**VI–VII.
22. **Edwards, E. A., L. E. Wills, M. Reinhard, and D. Grbic-Galic.** 1992. Anaerobic degradation of toluene and xylene by aquifer microorganisms under sulfate-reducing conditions. *Appl. Environ. Microbiol.* **58:**794–800.
23. **Engesgaard, P., and K. L. Kipp.** 1992. A geochemical transport model for redox-controlled movement of mineral fronts in groundwater flow systems: a case of nitrate removal by oxidation of pyrite. *Water Resource Res.* **28:**2829–2843.
24. **Essaid, H. I., B. A. Bekins, E. M. Godsy, E. Warren, M. J. Baedecker, and I. M. Cozarelli.** 1995. Simulation of aerobic and anaerobic biodegradation processes at a crude-oil spill site. *Water Resource Res.* **31:**3309–3327.
25. **Essaid, H. I., W. N. Herkelrath, and K. M. Hess.** 1993. Simulation of fluid distributions observed at a crude-oil spill site incorporating hysteresis, oil entrapment, and spatial variability of hydraulic properties. *Water Resource Res.* **29:** 1753–1770.
26. **Fetter, C. W.** 1999. *Contaminant Hydrogeology,* 2nd ed. Prentice-Hall, Englewood Cliffs, N. J.
27. **Franzmann, P. D., L. R. Zappia, T. R. Power, G. B. Davis, and B. M. Patterson.** 1999. Microbial mineralisation of benzene and characterisation of microbial biomass in soil above hydrocarbon contaminated groundwater. *FEMS Microbiol. Ecol.* **30:**67–76.
28. **Freeze, R. A., and J. A. Cherry.** 1979. *Groundwater.* Prentice-Hall, Englewood Cliffs, N. J.
29. **Griffiths, S. K., R. H. Nilson, and R. W. Bradshaw.** 1997. *In situ* bioremediation: a network model of diffusion and flow in granular porous media. SAND97-8250. Sandia National Laboratories, Albuquerque, N. Mex. http://infoserve.sandia.gov.
30. **Ham, R. J. Schotting, H. Prommer, and G. B. Davis.** 2004. Effects of hydrodynamic dispersion on plume lengths for instantaneous bimolecular reactions. *Adv. Water Resource* **27:**803–813.
31. **Hartog, N., J. Griffioen, and C. H. Van Der Weijden.** 2002. Distribution and reactivity of O_2-reducing components in sediments from a layered aquifer. *Environ. Sci. Technol.* **36:**2436–2442.
32. **Hartog, N., P. F. van Bergen, J. W. de Leeuw, and J. Griffioen.** 2004. Reactivity of organic matter in aquifer sediments: geological and geochemical controls. *Geochim. Cosmochim. Acta* **68:**1281–1292.
33. **Herzer, J., and W. Kinzelbach.** 1989. Coupling of transport and chemical processes in numerical transport models. *Geoderma* **44:**115–127.
34. **Istok, J. D.** 1989. Groundwater modeling by the finite element method. Water Resources Monograph no. 13. American Geophysical Union, Washington, D.C.
35. **Kindred, J. S., and M. A. Celia.** 1989. Contaminant transport and biodegradation. 2. Conceptual model and test simulation. *Water Resource Res.* **25:**1149–1160.
36. **Kinzelbach, W., W. Schäfer, and J. Herzer.** 1991. Modeling of natural and enhanced denitrification processes in groundwater. *Water Resource Res.* **27:**1123–1135.
37. **Kipp, K. L., Jr.** 1987. *HST3D—A Computer Code for Simulation of Heat and Solute Transport in 3D Ground-Water Flow Systems.* U.S. Geological Survey Water-Resources Investigations report 86-4095. U.S. Geological Survey, Reston, Va.
38. **Lawrence, J. R., and M. J. Hendry.** 1996. Transport of bacteria through geologic media. *Can. J. Microbiol.* **42:**410–422.
39. **Lu, G., T. C. Clement, C. Zheng, and T. H. Wiedemeier.** 1999. Natural attenuation of BTEX compounds: model development and field-scale application. *Ground Water* **37:**707–717.
40. **McDonald, J. M., and A. W. Harbaugh.** 1988. *A Modular 3D Finite-Difference Ground-Water Flow Model.* Techniques of Water-Resources Investigations report TWI 06-A1. U.S. Geological Survey, Reston, Va.
41. **Michaelis, L., and M. L. Menten.** 1913. Die Kinetik der Invertinwerkung. *Biochem. Z.* **49:** 333–369.

42. **Monod, J.** 1949. The growth of bacterial cultures. *Annu. Rev. Microbiol.* **3:**371–394.
43. **Parkhurst, D. L., D. C. Thorstenson, and L. N. Plummer.** 1980. *PHREEQE—A Computer Program for Geochemical Calculations.* U.S. Geological Survey. Water-Resources Investigations report 80-96. U.S. Geological Survey, Reston, Va.
44. **Parkhurst, D. L.** 1995. *User's Guide to PHREEQC—a Computer Program for Speciation, Reaction-Path, Advective-Transport, and Inverse Geochemical Calculations.* U.S. Geological Survey Water-Resources Investigations report 4227. U.S. Geological Survey, Reston, Va.
45. **Parkhurst, D. L., and C. A. J. Appelo.** 1999. *User's Guide to PHREEQC—A Computer Program for Speciation, Reaction-Path, 1D-transport, and Inverse Geochemical Calculations.* U.S. Geological Survey Water-Resources Investigations report 99-4259. U.S. Geological Survey, Reston, Va.
46. **Pinder, G. F., and W. G. Gray.** 1977. *Finite Element Simulation in Surface and Subsurface Hydrology.* Academic Press, London, U.K.
47. **Postma, D., and R. Jakobsen.** 1996. Redox zonation: equilibrium constraints on the Fe(III)/SO_4-reduction interface. *Geochim. Cosmochim. Acta* **60:**3169–3175.
48. **Prommer, H., G. B. Davis, and D. A. Barry.** 1999. Geochemical changes during biodegradation of petroleum hydrocarbons: field investigations and biogeochemical modeling. *Org. Geochem.* **30:**423–435.
49. **Prommer, H., D. A. Barry, and C. Zheng.** 2003. MODFLOW/MT3DMS-based reactive multicomponent transport modeling. *Ground Water* **41:**247–257.
50. **Prommer, H., D. A. Barry, and G. B. Davis.** 2002. Influence of transient groundwater flow on physical and reactive processes during biodegradation of a hydrocarbon plume. *J. Contam. Hydrol.* **59:**113–132.
51. **Rifai, H. S., P. B. Bedient, R. C. Borden, and J. F. Haasbeek.** 1987. *BIOPLUME II: Computer Model of Two-Dimensional Contaminant Transport under the Influence of Oxygen Limited Biodegradation in Ground Water Users' Manual.* Rice University, Houston, Tex.
52. **Rifai, S. H., and P. B. Bedient.** 1990. Comparison of biodegradation kinetics with an instantaneous reaction model for groundwater. *Water Resources Res.* **26:**637–645.
53. **Rittmann, B. E., and J. M. van Briesen.** 1996. Microbiological processes in reactive modeling, p. 311–334. *In* P. C. Lichtner, C. I. Steefel, and E. H. Oelkers (ed.), *Reactive Transport in Porous Media. Reviews in Mineralogy*, vol. 34. Mineralogical Society of America, Washington, D.C.
54. **Robertson, W. J., P. D. Franzmann, and B. J. Mee.** 2000. Spore-forming, Desulfosporosinus-like sulphate-reducing bacteria from a shallow aquifer contaminated with gasoline. *J. Appl. Microbiol.* **88:**248–259.
55. **Schäfer, D., W. Schäfer, and W. Kinzelbach.** 1998. Simulation of processes related to biodegradation of aquifers. 2. Structure of the 3D transport model. *J. Contam. Hydrol.* **31:**167–186.
56. **Steefel, C. I., and K. T. B. MacQuarrie.** 1996. Approaches to modeling of reactive transport in porous media, p. 83–129. *In* P. C. Lichtner, C. I. Steefel, and E. H. Oelkers (ed.), *Reactive Transport in Porous Media. Reviews in Mineralogy*, vol. 34. Mineralogical Society of America, Washington, D.C.
57. **Thierrin, J., G. B. Davis, and C. Barber.** 1995. A ground water tracer test with deuterated compounds for monitoring in situ biodegradation and retardation of aromatic hydrocarbons. *Ground Water* **33:**469–475.
58. **Thullner, M., and W. Schäfer.** 1999. Modeling of a field experiment on bioremediation of chlorobenzenes in groundwater. *Bioremed. J.* **3:**247–267.
59. **Van Briesen, J. M., and B. E. Rittmann.** 2000. Mathematical description of microbial reactions involving intermediates. *Biotechnol. Bioeng.* **67:** 35–52.
60. **Van Cappellen, P., J.-F. Gaillard, and C. Rabouille.** 1993. Biogeochemical transformations in sediments: kinetic models of early diagenesis, p. 401–447. *In* R. Wollast, F. T. Mackenzie, and L. Chou (ed.), *Interactions of C, N, P and S—Biogeochemical Cycles and Global Change.* Springer-Verlag, Berlin, Germany.
61. **Walter, A. L., E. O. Frind, D. W. Blowes, C. J. Ptacek, and J. W. Molson.** 1994. Modeling of multi-component reactive transport in groundwater. 1. Model development and evaluation. *Water Resource Res.* **30:**3137–3148.
62. **Wang, H., and M. Anderson.** 1982. *Introduction to Groundwater Modeling: Finite Difference and Finite Element Methods.* W. H. Freeman and Co., New York, N.Y.
63. **Watson, I. A., S. E. Oswald, K. U. Mayer, Y. Wu, and S. A. Banwart.** 2003. Modeling kinetic processes controlling hydrogen and acetate concentrations in an aquifer-derived microcosm. *Environ. Sci. Technol.* **37:**3910–3919.
64. **Wiedemeier, T. H., J. T. Wilson, D. H. Kampbell, R. N. Miller, and J. E. Hansen.** 1995. *Technical Protocol for Implementing Intrinsic Remediation with Long-Term Monitoring for Natural Attenuation of Fuel Contamination Dissolved in Groundwater.* Technology Transfer Divisions 1 & 2, Air Force Center for Technical Excellence. Brooks Air Force Base, San Antonio, Tex.
65. **Yeh, G. T., S. Sharp-Hansen, B. Lester, R.**

Strobl, and J. Scarbrough. 1992. *Three-Dimensional Finite Element Model of Water Flow through Saturated-Unsaturated Media (3DFEMWATER)/ Three-Dimensional Lagrangian-Eulerian Finite Element Model of Waste Transport through Saturated-Unsaturated Media (3DLEWASTE): Numerical Codes for Delineating Wellhead Protection Areas in Agricultural Regions Based on the Assimilative Capacity Criterion.* EPA report/600/R-92/223. Environmental Protection Agency, Athens, Ga.

66. **Yeh, G. T., and V. S. Tripathi.** 1989. A critical evaluation of recent developments in hydrogeochemical transport models of reactive multichemical components. *Water Resource Res.* **25:** 93–108.
67. **Zheng, C., and P. P. Wang.** 1999. *MT3DMS: a Modular Three-Dimensional Multispecies Transport Model for Simulation of Advection, Dispersion and Chemical Reactions of Contaminants in Groundwater Systems.* Documentation and user's guide, contract report SERDP-99-1. U.S. Army Engineer Research and Development Center, Vicksburg, Miss.
68. **Zheng, C., and Bennett.** 2002. *Applied Contaminant Transport Modeling,* 2nd ed. Wiley, New York, N.Y.
69. **Zysset, A., F. Stauffer, and T. Dracos.** 1994. Modeling reactive groundwater transport governed by biodegradation. *Water Resources Res.* **30:** 2435–2448.